Geochemistry Geophysics Geosystems G3
AN ELECTRONIC JOURNAL OF THE EARTH SCIENCES
Published by AGU and the Geochemical Society

Article
Volume 6, Number 1
20 January 2005
Q01003, doi:10.1029/2004GC000814
ISSN: 1525-2027

MiFil: A method to characterize seafloor swells with application to the south central Pacific

Claudia Adam, Valerie Vidal, and Alain Bonneville

Laboratoire de Géosciences Marines, Centre National de la Recherche Scientifique, Institut de Physique du Globe, 4 Place Jussieu, Paris 75252, France (bonnevil@ipgp.jussieu.fr)

[1] We propose a filtering method to characterize large-scale depth anomalies. The MiFil method (for minimization and filtering) requires two stages: a first one to roughly remove the volcano component by minimizing the depth anomaly and a second one to smooth the shape and totally remove the small spatial length scale remaining topography using a median filter. The strength of this method, directly applicable on two-dimensional grids, is that it does not require any assumption on the location, amplitude, or width of the large-scale feature to characterize, except its minimal width. We only consider the spatial length scale of the features to remove. Application to volcanic chains of the south central Pacific is presented, and the results lead to a better understanding of the tectonics and volcanism emplacement of the zone. The Society is the only "classical" hot spot that corresponds to the simple interaction of a plume with the lithosphere and for which a buoyancy flux of 1.58 ± 0.15 Mg s^{-1} is obtained. The Marquesas volcanic chain, although quite comparable, presents a swell morphology that prevents such interpretation and quantification. For the Tuamotu and Cook-Austral volcanic chains, no reliable quantification can be made because the depth and geoid anomalies are caused by several phenomena occurring at different depths that cannot be separated.

Components: 10,161 words, 19 figures, 1 table.

Keywords: depth anomaly; hot spot; spatial filter; swells.

Index Terms: 0910 Exploration Geophysics: Data processing; 3037 Marine Geology and Geophysics: Oceanic hotspots and intraplate volcanism; 3045 Marine Geology and Geophysics: Seafloor morphology, geology, and geophysics; 9355 Geographic Location: Pacific Ocean.

Received 10 August 2004; **Revised** 25 October 2004; **Accepted** 9 December 2004; **Published** 20 January 2005.

Adam, C., V. Vidal, and A. Bonneville (2005), MiFil: A method to characterize seafloor swells with application to the south central Pacific, *Geochem. Geophys. Geosyst.*, *6*, Q01003, doi:10.1029/2004GC000814.

1. Introduction

[2] Variations in seafloor depth with age when the oceanic lithosphere spreads away from mid-ocean ridges reflects at first order the cooling and sinking of a plate when moving away from a hot boundary [*Turcotte and Oxburgh*, 1967; *Sclater and Francheteau*, 1970]. However, bathymetric features can regionally depart from the subsidence models describing this conductive cooling [*Parker and Oldenburg*, 1973; *Parsons and Sclater*, 1977]. The corresponding depth anomalies map [*Menard*, 1973] is obtained by substracting the expected depth based on crustal age from the observed depth. It displays anomalies of different spatial length scales: the volcanic edifices (~100 km), wide shallow regions around hot spots [*Wilson*, 1963; *Morgan*, 1971], called swells (~1000 km) and huge shallow regions (several thousand kilometers) as the South Pacific Superswell [*McNutt and Fischer*, 1987; *Sichoix et al.*, 1998].

[3] A precise characterization of hot spot swells is required in order to understand the phenomena at the origin of these anomalies. Moreover, their

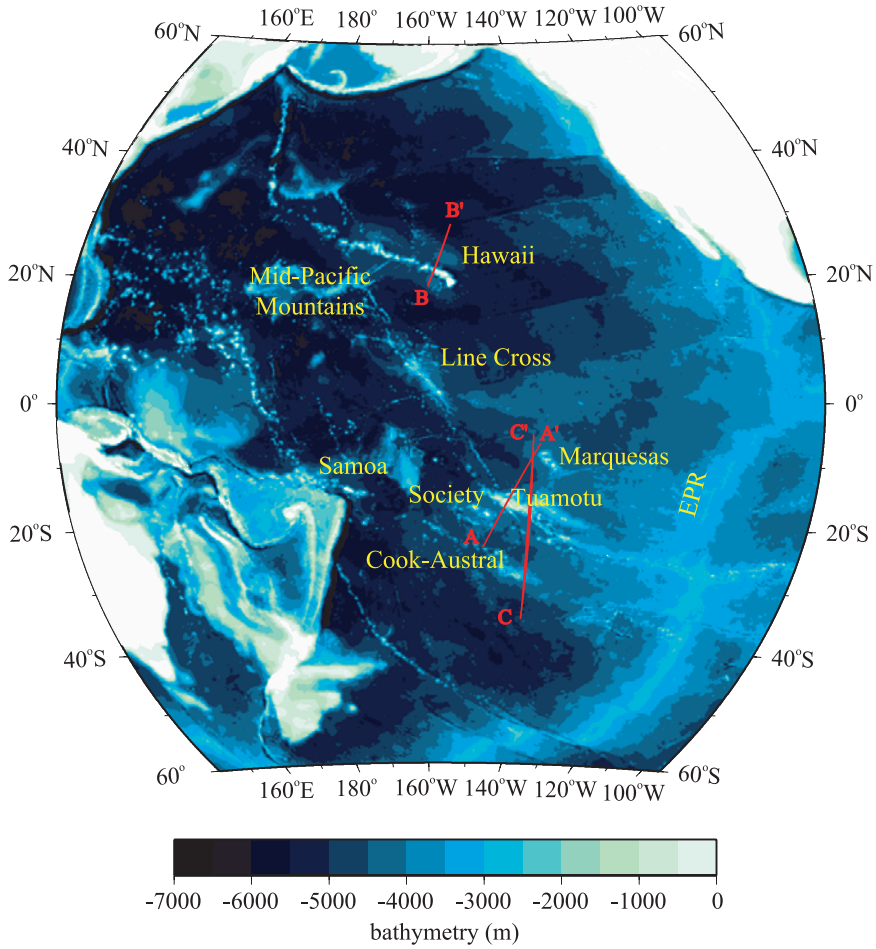

Figure 1. Bathymetry of the Pacific, from *Smith and Sandwell* [1997], version 8.2. Profiles AA′, BB′, and CC′ are discussed in the text.

precise description is necessary to have reliable quantification, such as the flow of material from the mantle, which helps to distinguish deep plumes from more superficial ones. The south central Pacific (Figure 1) is a region well-known for its high concentration of volcanism and its complex tectonic history. In this region, many phases of volcanism are often superimposed on the same alignment. One alignment could thus present several swells.

[4] This hypothesis cannot be checked by the modal analysis [*Crough*, 1983] previously used on this region [*Sichoix et al.*, 1998]. In another attempt to approximate the profile of a swell topography, *Wessel* [1993] used super-Gaussian transversal to the hot spot track. This approach needs two strong hypotheses: the shape of the swell and its emplacement along the volcanic chain. We demonstrate in this study that these characteristics are not systematic. Moreover, the swells are superimposed on the South Pacific Superswell and these two contributions have never been clearly separated, leading to a bad estimation of the swells amplitude in this region with severe consequences for the interpretation. For example, an uncertainty of 100 m on a swell amplitude can lead to an error of 60°C on the thermal structure of the underlying plume [*Sleep*, 1990].

[5] In order to study the south central Pacific region, we have developed a nonspectral method able to characterize and isolate seafloor swells. Although it has already been recently used [*Vidal and Bonneville*, 2004], this method has not yet been precisely described nor compared to the existing "traditional" filtering techniques. The complete description of this method is one of the main purposes of the present paper. The MiFil method (for minimization and filtering) does not require any assumption on the emplacement, shape or extension of the anomalies to

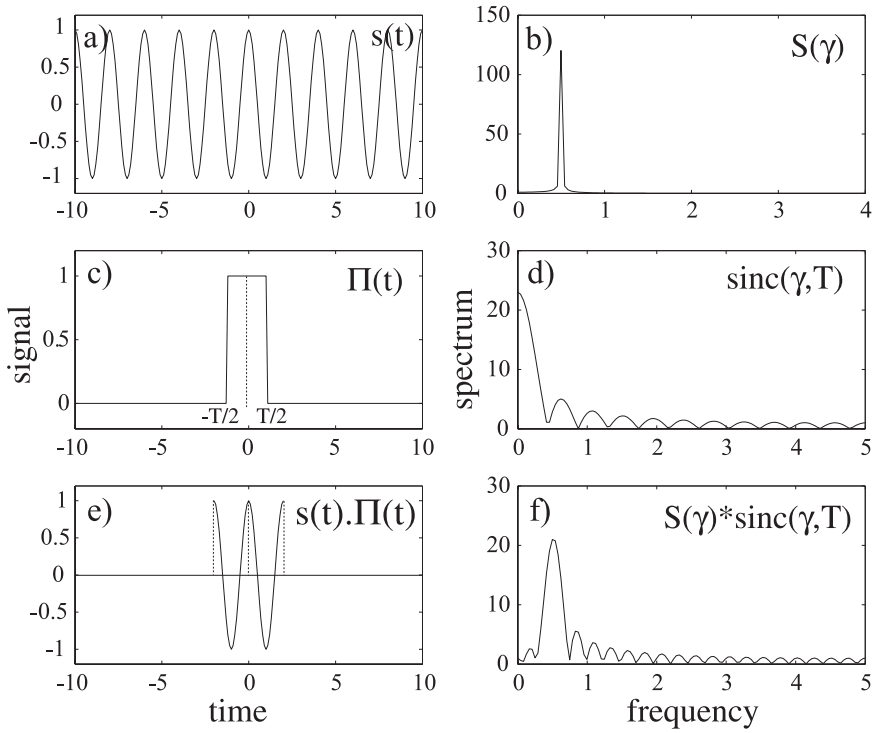

Figure 2. Illustration of the consequences of the finite nature of a periodic signal on the spectral domain. (a) Periodic function *s* (cosine, period 2) and (b) its sharp spectrum. (c) Window function Π used to shorten the signal to two periods. (d) Its spectrum is a cardinal sine function. (e) Truncated periodic signal, and (f) its spectrum: the energy is partially distributed toward neighboring frequencies.

describe, which makes it a reliable way to investigate the complex area of the south central Pacific.

2. Regional-Residual Separation of Geophysical Data

[6] Many geophysical data sets consist of a variety of different length-scale features. In order to analyze and interpret them, these different length-scale phenomena need to be separated. This process, referred to as regional-residual separation [*Telford et al.*, 1986], has generated many filtering methods. The next section presents a review of the most commonly employed methods and lists their shortcomings. The existing filtering techniques can be classified into three main categories: spectral filtering, adjustment of the anomaly by a mathematical surface, or spatial filtering.

[7] To discuss these different filtering methods, we have chosen to apply them on on several profiles extracted from the bathymetry grid of *Smith and Sandwell* [1997] version 8.2. But for the quantitative studies presented in section 4, we have used a more adequate data set, which will be presented further.

2.1. Traditional Filtering Techniques

2.1.1. Spectral Filtering

[8] Because of the presence of different spatial length scales in the data sets, low-pass convolutive filters have often been used [*Watts and Daly*, 1981; *Ribe and Watts*, 1982; *Watts et al.*, 1985; *Cazenave and Dominh*, 1987]. However, the finite and nonperiodic characteristics of most geophysical observations can introduce a important bias in the regional-residual separation. The problem of a finite signal is illustrated in Figure 2. The spectrum associated with a periodic signal (Figure 2a), with a well-defined frequency is shown in Figure 2b. The sharp peak indicates the right frequency: 0.5. If we isolate a part of this signal by convolution with a window function (Figures 2c, 2d, 2e) [*Bendat and Piersol*, 1986], we point out the most important problem of finite signal filtering (Figure 2f): the leakage of a given frequency toward the neighboring frequencies.

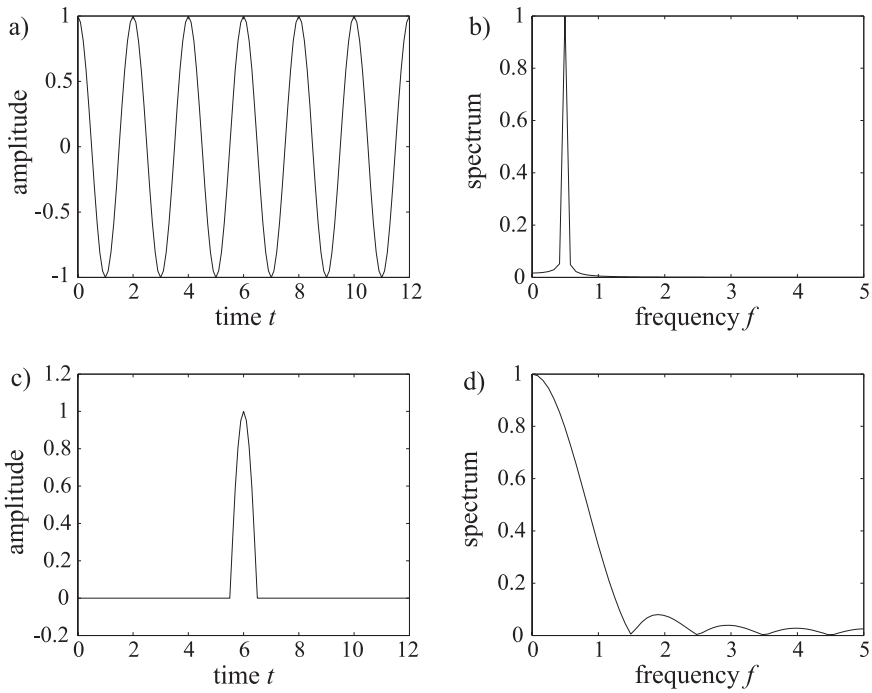

Figure 3. Spectrum computation of a periodic and a nonperiodic signal. (a) Periodic function (cosine, periodicity 2, dashed line) and (c) nonperiodic function (cosine arch). (b) Spectrum of the periodic function and (d) spectrum of the cosine arch.

[9] This effect can be strongly attenuated by using convolutive windows with a different and smoother spectral signature, such as Gaussian windows. The Gaussian convolutive filtering has therefore been one of the most used convolutive filtering in data analysis. However, even if in a lesser way than the above example, it still deteriorates the initial signal, and makes the spectral analysis somehow biased. The second important shortcoming of the spectral filtering is that this method assumes that features of interest have most of their spectral power at wavelengths not strongly represented in the background field. This strong hypothesis is not always checked, due to the frequent wavelength range overlapping between regional and residual features [*Wessel*, 1998]. Moreover, even when assuming that the phenomena have nonoverlapped spectral ranges, their existence as finite and nonperiodic series introduces a strong bias in their characterization.

[10] This is illustrated in Figure 3, where are plotted a periodic signal (cosine function) and a single cosine arch, and their associated spectra. In the periodic case, the spectrum indicates the wavelength of the original signal. In the nonperiodic case, however, the frequency peak is shifted toward a much lower frequency. In particular, bathymetry can have isolated features whose shape can be roughly approximated by an arch. For a geographical restricted zone, a bathymetric feature which is not repeated enough times to have a significant spectral signature will not appear at the correct frequency in the spectral domain. All these considerations illustrate the fact that the term "wavelength" is not appropriate for bathymetric features and we will prefer to use "spatial length-scale" in order to avoid any misunderstanding. Finally, a last and important shortcoming of the spectral filters has to be discussed. Convolutive filters only manipulate the amplitudes of the data's sinusoidal components, meaning that the residual function integrates to zero. In particular, the use of such filters to separate the swell component from topography associated with volcanism, in the case of a hot spot chain, hinders any further volume computation. Figure 4 illustrates the problems linked to the use of convolutive filters. We have filtered the depth anomaly grid along the profile shown in Figure 1, in order to isolate the regional (swell) component.

[11] No satisfying compromise can be found between the fitting wavelength and amplitude. Therefore spectral filtering is not adapted to depth anomalies characterization.

2.1.2. Geometrical Methods

[12] An alternative method consists in estimating the regional depth by a mathematical shape. Swells

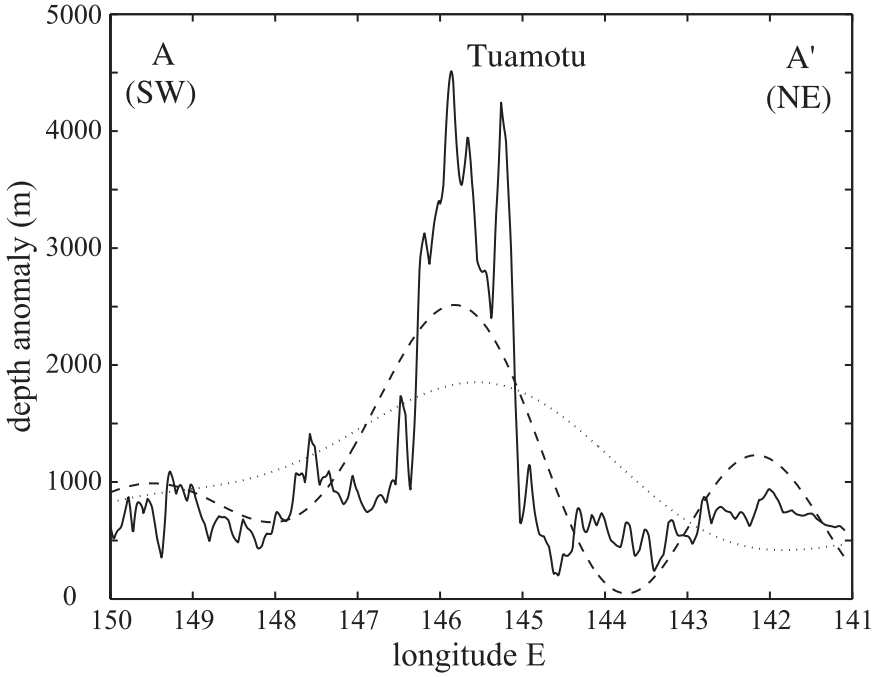

Figure 4. Swell determination in the Tuamotu region by spectral filtering (profile AA′ located in Figure 1). The depth anomaly (solid line) is filtered with convolutive filters of cut-off wavelength 100 km (dashed) and 200 km (dotted).

have been first approximated as Gaussian functions [*Crough*, 1978] in the direction perpendicular to the hot spot chain. On the basis of theoretical [*Huppert*, 1982] and experimental [*Didden and Maxworthy*, 1982] studies, predicting a swell flattening, *Wessel* [1993] proposed to fit the topographic swells by super-Gaussians:

$$f(x) = h_0 \exp\left(-\left|\frac{x}{w}\right|^p\right), \quad (1)$$

where h_0 is the swell amplitude, w is the standard deviation, and p determines the curve shape ($p = 2$ is the Gaussian case).

[13] Figure 5 shows the determination of the Hawaiian hot spot swell with the geometrical method. This method seems more accurate than the spectral method, for it does not overestimate the swell amplitude. However, many shortcomings are also associated with this method. First, it works on profiles, and is not directly applicable on two-dimensional grids. Second, the simultaneous nonlinear adjustment of the five parameters (h_0, w, center of the super-Gaussian, regional depth and slope) has to be done on the flanks of the depth anomaly, in order not to take into account the topography associated with volcanism. The choice of the fitting region remains subjective. Third, this method assumes a strong hypothesis: the swell has to be symmetrically developed on each side of the main alignment. This is not always checked, and indeed is not the case for the south central Pacific swells, as we will show in section 4. Finally, the choice of a super-Gaussian shape has no physical signification, and therefore remains a purely convenient graphical fitting method.

2.1.3. Spatial Filtering

[14] Filters in the spatial domain are based on the fact that geophysical data of a given length scale usually contains many wavelengths, due to their complex topography [*Wessel*, 1998]. Indeed, these nonlinear filters do not have a spectral representation. They work directly on the spatial length scales of features, and not their spectral component, and so provide a much better separation of the regional and residual components (swell and seamounts for bathymetry, respectively). The most used among them are the mean, median and mode filters.

[15] Figure 6 shows the determination of the Tuamotu swell with different spatial filters. The mean filtering also tends to overestimate the broad features amplitude, and is the less appropriate for the regional and residual components separation. The modal filter, introduced by *Crough* [1978], has been extensively used to find the swell characteristics, in particular in French Polynesia, where

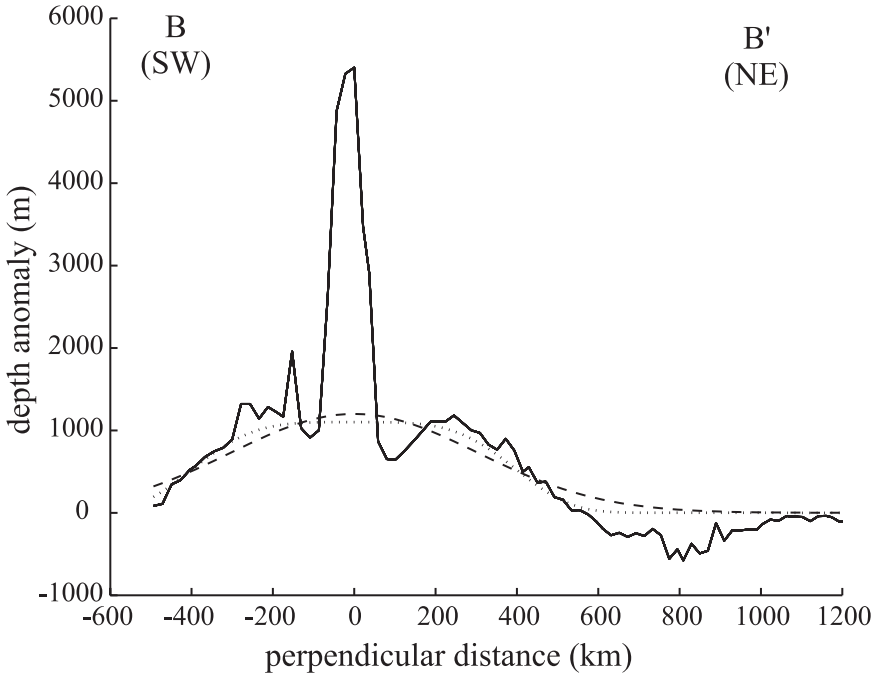

Figure 5. Swell determination with the geometrical method for the Hawaiian hot spot (profile BB′ indicated in Figure 1). Depth anomaly is the solid black line. Its regional component is adjusted by a Gaussian (dashed) or a super-Gaussian (dotted, $p = 4$).

Sichoix et al. [1998] determined the swells and Superswell amplitudes. However, this approach supposes the knowledge of the regional anomaly axial spreading. Moreover, it can introduce an overestimation of the swell amplitude near the hot spot trend, because of the influence of the volcanic edifices topography [*Adam*, 2003]. *Smith* [1990] demonstrates that the median filter is better

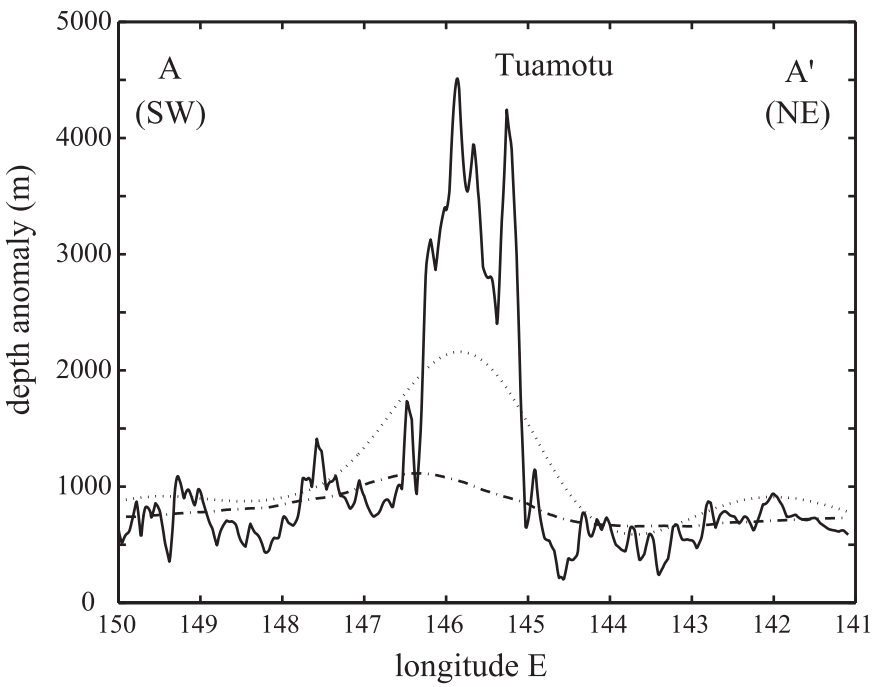

Figure 6. Swell determination with spatial filters for the Tuamotu (profile AA′ indicated in Figure 1). Depth anomaly is the solid black line. Its regional component is adjusted by a median (dotted) and a mean (dashed-dotted) filter.

than the modal one, for it is less noisy and more convenient to compute. Median filters return the median value inside the filtering window. In Figure 6 the profile associated with the median filtering is plotted for the Tuamotu swell. This is the best fitting one among the spatial filters. It is particularly well adapted to bathymetry, which includes steep features like fracture zones [*Smith*, 1990]. Indeed, because of its ability to ignore the presence of values far from the typical one, it makes it possible to completely eliminate features [*Wessel*, 1998]. The insensibility to extreme values is the characteristics of robust estimators [*Rousseeuw and Leroy*, 1987].

[16] The median filter is therefore the best filtering method among all the classical filtering techniques. However, as shown in Figure 6, it still does not fit the regional component as expected, and tends to slightly overestimate the regional depth component in the vicinity of the volcanic edifices. Moreover, if the reference seafloor is not perfectly flat, with for instance seamounts distributed not symmetrically around the seafloor level, or a sloping background, then the median will be biased toward shallow values [*Smith*, 1990; *Wessel*, 1998].

2.2. MiFil Method

[17] In order to efficiently remove all topographic features smaller than a given spatial length scale, we have elaborated a new filtering method. On the basis of the previous discussion, we know that the spatial filters (and in particular the median one) are the most adapted for the regional-residual separation, but still overestimate the regional depth component, for they do not remove efficiently enough the volcanic edifices contribution to topography. One more stage has then to be added. The method presented here is based on the two following stages: the first stage minimizes the original grid, in order to roughly remove the volcanic edifices contributions, and the second stage sweeps the resulting grid with a median filter, in order to smooth the previous grid and definitely eliminate the volcanic edifices contributions. This method, hereafter called MiFil (minimization and filtering), is a good method for regional-residual separation [*Vidal and Bonneville*, 2004]. Details of the two stages are described below.

2.2.1. First Stage: Minimization

[18] The first stage of MiFil (minimization) consists in minimizing the depth anomaly grid [*Vidal and Bonneville*, 2004]. We improve the method by using a circular minimizing filter instead of squared one, which is physically more consistent. Around each point of the input grid, one sweeps a region of radius r (r being a constant in km). For each step, the new value taken for the resulting minimized grid at the center of the disk corresponds to the minimum of the depth anomaly found in that swept area.

[19] If λ_c is the maximum topographic length to eliminate, the radius r of the minimizing disk has to be

$$r \sim \lambda_c/4. \tag{2}$$

A compromise has to be found on the r value. Indeed, any local minimum value in the original depth anomaly grid will be spread on a $4r$ circular region. A too large r value could therefore extend over an unwanted area some minimal values such as those introduced by fracture zones, and therefore introduce an important error on the regional depth estimation. Figure 7, stage I, shows two profiles extracted from the minimized grid with different disk radii r. Observe in particular the minimized curve in the vicinity of the Marquesas fracture zone. In both cases, the small spatial length scale features are flattened but not completely removed.

2.2.2. Second Stage: Filtering

[20] The second stage of MiFil (filtering) smooths the shape and totally removes the small spatial length scale remaining topography. We use a median filter from the Generic Mapping Tools (GMT) software [*Wessel and Smith*, 1991]. This filter considers for each point of the input grid a disk of diameter $2R$ centered on that point. The filtered value of the output grid is the median of all points found inside this disk. The disk is then swept through the grid. The median measures the central tendency: it smooths the minimized grid, and removes the remaining small spatial length scale topographic features. Outliers like minima associated with fracture zones have little effect on it. It was thus preferred to the mean value, which is too much influenced by seamounts' topography and is thus unable to remove it completely. The condition to completely remove a length scale λ is [*Wessel*, 1998]

$$R \geq \sqrt{2}\lambda. \tag{3}$$

However, if R is taken too large, large spatial length scales will also be removed. We explore a

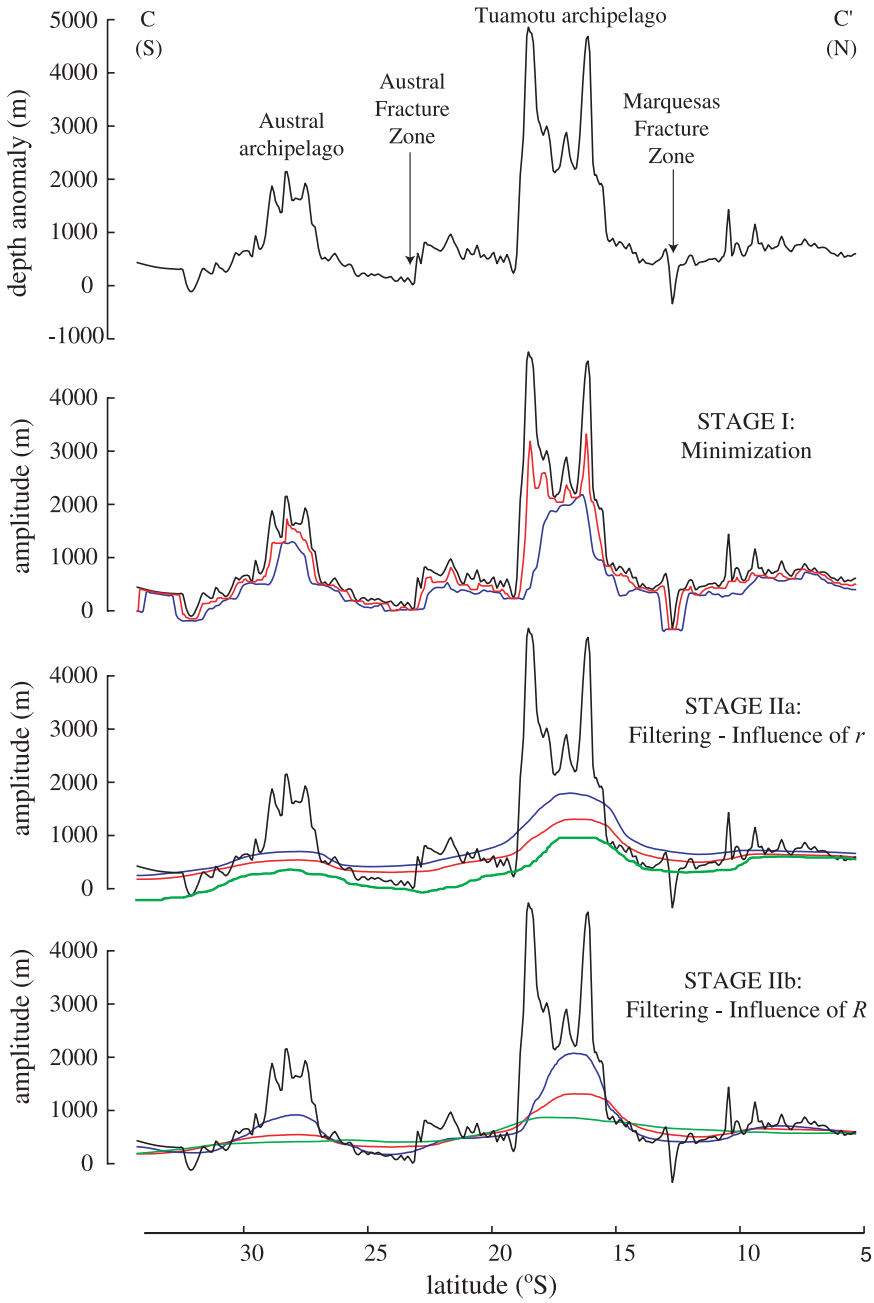

Figure 7. The top black line represents a profile of depth anomaly at longitude 217.8°E (profile CC′, Figure 1). Stage I, minimization with different disk radii: r = 20 km (red) and r = 50 km (blue). Stage IIa, minimization with r = 5 km (blue), r = 15 km (red), and r = 70 km (green), and filtering with R = 350 km. Stage IIb, minimization with r = 15 km and filtering with R = 200 km (blue), R = 350 km (red), and R = 500 km (green).

physically acceptable range of this parameter (close to $\sqrt{\lambda}$) in order to check its influence.

2.2.3. Influence of the Parameters (r, R)

[21] The MiFil method can be directly applied to two-dimensional (2-D) depth anomaly grids. Its strength lies on the fact that no assumption is required on the location or width of the depth anomaly to be characterized. Therefore it is applicable to depth anomaly characterization of different spatial length scales, like hot spot swells [*Vidal and Bonneville*, 2004] or the South Pacific Superswell (C. Adam and A. Bonneville, New extent for the South Pacific Superswell, submitted to *Journal of Geophysical Research*, 2004; hereinafter referred to as Adam and Bonneville, submitted manuscript, 2004). In this study, we have used it to precisely

determine the swells characteristics in French Polynesia (Pacific). It is important, before any discussion concerning the swells shape and amplitudes, to test the robustness of the method. It has been done by analyzing the influence of the MiFil parameters: the radii of the minimizing filter r and of the median filter R.

[22] The radius r of the minimizing disk is taken between 5 and 70 km: below 5 km the depth anomaly is not sufficiently filtered and above 70 km the fracture zones influence is too widened. Figure 7, stage IIa, shows the influence of the size of the minimizing windows on the final result. Disk of radii 5, 15 and 70 km are used for minimization. All of resulting minimized grids are filtered afterward with the same R = 350 km median filter. The r = 5 km minimizing disk overestimates the Tuamotu swell: the grid is not minimized enough. The median filtering amplifies this lack of minimization by shifting up the final profile. On the contrary, the r = 70 km minimizing disk underestimates the swell amplitude by spreading the local minimal values associated in particular with fracture zones. The r = 15 km minimizing disk fits well the swell shape, and removes efficiently the volcanic features associated with the hot spot activity. All these parameters are specific to the Tuamotu swell. The best fitting parameters have to be determined for each studied large spatial length scale anomaly.

[23] *Wessel* [1993] and *Sichoix* [1997] indicate spatial scales between 500 and 1000 km for the swells. Moreover, volcanic edifices have a maximum spatial scale of about 150 km (Tuamotu). We thus considered radii R of the order of a hundred kilometers (see equation (3)) for the median filter. The analysis of the influence of the median filter radius R is shown in Figure 7, stage IIb. Stage I is performed with a r = 15 km minimizing disk and filtered with R = 200, 350 and 500 km median filter radius. For the lowest values of the radius (200 km), the contribution of the volcanoes is not totally removed from the Tuamotu swell. For the highest values (R = 500 km) we obtain a large spatial length scale filtered depth anomaly not related to the local swells anymore. The best fitting parameters for the Tuamotu swell are thus r = 15 km and R = 350 km.

[24] The reliability of the MiFil method has been tested by computing for each swell the error associated with the choice of the parameters r and R. The maximum and minimum amplitudes are computed with the extrema r and R, within the physically acceptable range. The error is taken as the maximum difference between the swell amplitude and the minimal or maximal value. It does not exceed 10% of the swell amplitude.

2.2.4. Parameters (r, R) for the South Central Pacific Swells

[25] The best-fitting (r, R) parameters have been determined for each swell, with the above method. In order to find the local swell contribution to regional topography, we must first remove the South Pacific Superswell contribution.

[26] The green line in Figure 8 shows the best estimation of the Superswell (r = 50 km and R = 700 km) on a N-S profile crossing French Polynesia (see Figure 1). A complete study of the South Pacific Superswell characteristics is presented by Adam and Bonneville (submitted manuscript, 2004). After isolating the Superswell contribution, we have determined the best-fitting parameters for the local swells. Figure 8 displays the example of the Tuamotu and Austral swells, and illustrates once more the fact that the best-fitting MiFil parameters have to be determined independently for each studied large spatial length scale anomaly.

[27] In the next section, we use the MiFil method to characterize the hot spot swells in French Polynesia.

3. Data

[28] The hot spot swells in the South Pacific have been studied with the bathymetric and geoid data. In the following paragraphs, we discuss the data and the corrections we applied before filtering them.

3.1. Depth Anomaly

[29] First, we have computed the depth anomaly which is the difference between the observed bathymetry and a theoretical depth given by a model of thermal subsidence of the lithosphere. In this study, the observed bathymetry was elaborated from two grids. The first grid, from *Jordahl et al.* [2004], extends between latitudes 32 and 5°S and longitudes 130 and 160°W. It was elaborated using original single-beam and multibeam ship soundings. Regions without data have been completed by the predicted bathymetry of *Smith* [1993], the predicted data sets being adjusted for the long wavelength given by the ship soundings data. This grid does not include all the volcanic chains in the region and it is not large enough to

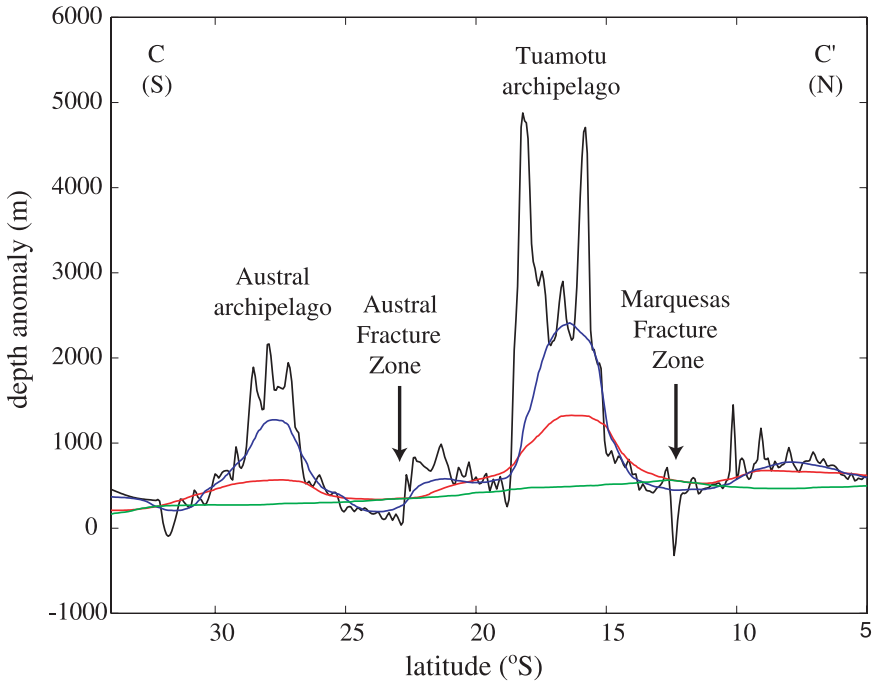

Figure 8. Swells and Superswell: the black line is the depth anomaly at longitude 217.8°E (see Figure 1). Parameters r = 15 km and R = 350 km best fit the Tuamotu swell (red); r = 10 km and R = 150 km best fit the Austral swell (blue); and r = 50 km and R = 700 km best fit the Superswell (green).

encompass the whole Superswell extent. We extended it to the latitude 20°N and longitude 170°W by adding original single-beam and multibeam ship soundings gathered with satellite navigation since 1973. This bathymetry map and the corresponding ship tracks are displayed in Figure 9. The coverage of the region is good and seems quite adequate for the determination of swells associated with volcanic alignments.

[30] We have corrected this bathymetry grid for sediment loading. The relation between the observed bathymetry (H) and the bathymetry corrected for sediment loading (H') is given by equation (4), where ρ_s, ρ_m and ρ_w are the densities of sediments, mantle and sea water, respectively, and h the sediment thickness compiled by the National Geophysical Data Center (NGDC):

$$H' = H - \left(\frac{\rho_s - \rho_m}{\rho_m - \rho_w}\right) h. \quad (4)$$

[31] The theoretical depth is given by thermal subsidence models which describe the evolution of the seafloor depth with age. To compute this theoretical depth (H_{theo}), we have used the global age grid of *Müller et al.* [1997] (version 1.3) and the GDH1 thermal subsidence model [*Stein and Stein*, 1992].

[32] As the Polynesian hot spots are superimposed on the South Pacific Superswell, we have to remove this component (H_{SS}) in order to have a correct estimation of the hot spot swell amplitude. To obtain this component, we elaborated a bathymetry grid from single-beam and multibeam ship soundings that we interpolated with the GMT surface and blockmedian functions [*Wessel and Smith*, 1991] into a $4' \times 4'$ grid. We then applied the same processing previously described: sediment correction, determination of the depth anomaly and filtering with the r = 50 km and R = 700 km parameters. The precise characterization of H_{SS} given by Adam and Bonneville (submitted manuscript, 2004) is used here.

[33] The depth anomaly (ΔH) we use hereafter is the difference between observed depth corrected for sediment loading (H' in equation (4)) and a theoretical depth predicted by the GDH1 subsidence model (H_{theo}), added to the Superswell component (equation (5)):

$$\Delta H = H' - H_{theo} - H_{SS}. \quad (5)$$

[34] We have then to remove the volcanoes contribution using the MiFil method. In order to avoid the influence of the neighboring alignments, we had to apply masks on each volcanic chain before

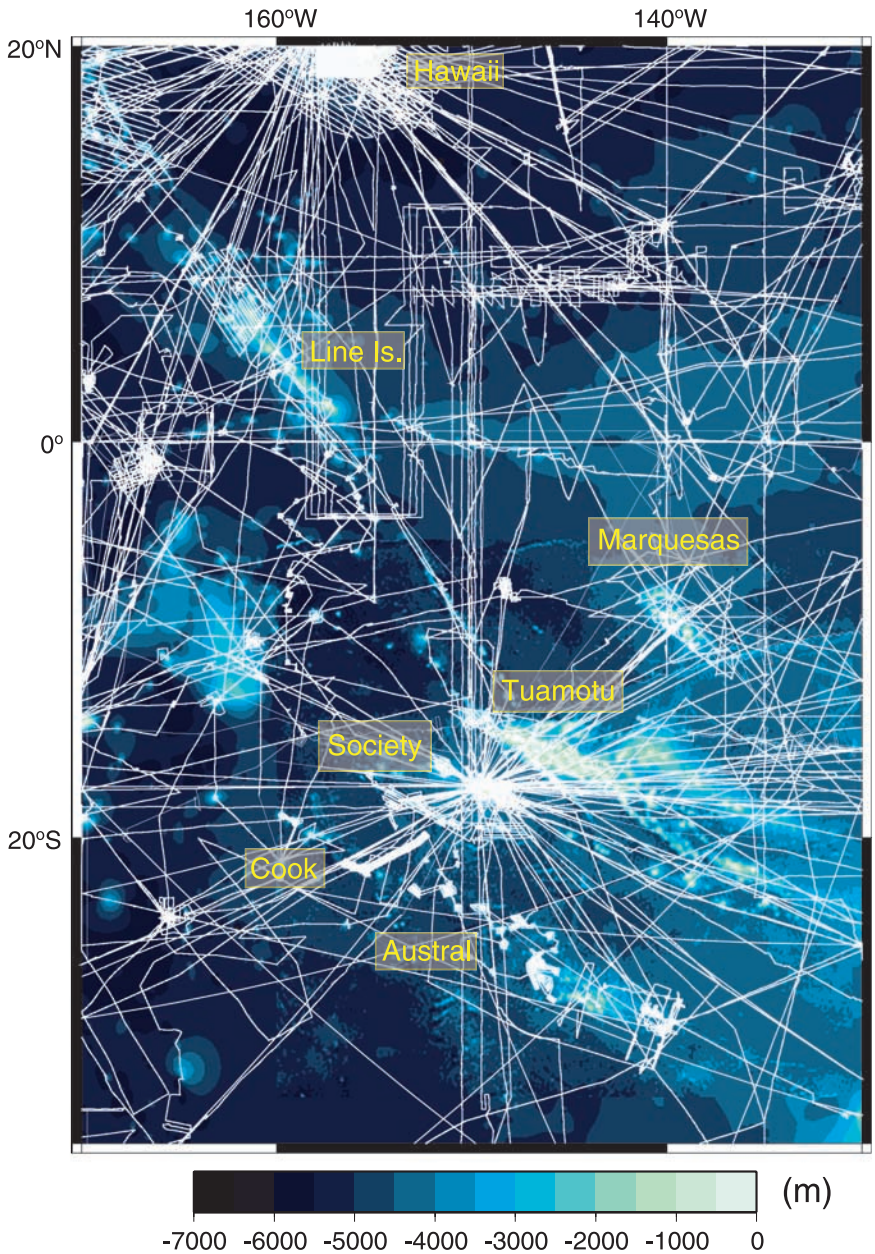

Figure 9. Bathymetry obtained from original ship soundings. The lines represent the ship tracks used in this compilation.

filtering. The filtering parameters are summarized in Table 1.

3.1.1. Buoyancy Flux

[35] The mass anomaly associated with the swell can be represented by the buoyancy flux. It quantifies the material flux from the mantle which creates the swell associated with hot spots [*Sleep*, 1990]. *Courtillot et al.* [2003] use it as a criterion to distinguish between deep plumes, which involve a buoyancy flux greater than 1 Mg s^{-1}, and more superficial plumes. It is represented by B with

$$B = WE(\rho_m - \rho_w)V_L, \quad (6)$$

where W is the swell's width, E its mean amplitude, ρ_m and ρ_w the mantle and sea water densities and V_L the plate velocity [*Davies*, 1988; *Sleep*, 1990].

[36] We compute the buoyancy flux for each alignment. Our values are summarized in Table 1. In the

Table 1. Filtering Parameters and Swells Characterization[a]

	Filtering		Swell Parameters					Volume/Fluxes (Volume/Buoyancy)		
	r, km	R, km	a, m	L, km	w, km	d_{av}, km	d_{comp}, km	$V \times 10^5$, km^3	V_f, m^3 s^{-1}	B, Mg s^{-1}
Society	15	150	980	900	500	215	40 ± 7	1.85	0.70 ± 0.07	1.58 ± 0.15
Marquesas	11	210	640	750	500	275	-	1.54	0.62[b]	1.42[b]
Tuamotu	15	350	890	600	1700	-	-	-	-	-
South Austral	10	150	1220	1250	500	373	20 ± 5	-	-	-
Cook (1)	15	175	410	600	600	220[c]	45 ± 5	1.54	0.41 ± 0.04	0.92 ± 0.09
Cook (2) N/S	5	120	580/560	500/650	250/400	-	-	-	-	-
Hawaii	-	-	1100	2800	1000	35	-	9.53	2.0 ± 0.7	4.7 ± 1.7

[a] Notes: a is the swell amplitude (with a 50 m uncertainty), L and w are the swell extensions in the longitudinal and transversal directions, respectively, d_{av} is the distance of the swell maximum from active volcanism, and d_{comp} is the compensation depth. V is the volume associated to the swell, and B is the buoyancy flux (see text).

[b] The fluxes for the Marsquesas are not reliable since they involve several phenomena. Their associated error is then hardly quantifiable (see text).

[c] Extrapolating the actual hot spot position from Rarotonga (1.1 Ma).

following sections, the results are discussed and interpreted for each volcanic chain.

3.2. Geoid

[37] To understand the phenomena at the origin of the depth anomalies, it is interesting to consider the geoid anomaly. The positive geoid anomalies indicate compensation by a density deficiency. The depth at which this compensation occurs for hot spots is generally about 50–100 km [*Crough*, 1978]. In this study, we have used a geoid grid, elaborated from ERS1-GM and GEOSAT data [*Mazzega et al.*, 1997] from which wavelengths greater than 2000 km have been filtered.

[38] We removed the volcanoes contribution by using the MiFil method. The filtering parameters are the same that those used to characterize the topographic swells. This approach is appropriate since at short spatial length scale, gravity anomalies correlate quite well with bathymetric features.

[39] Given the bathymetry and geoid anomaly, we can compute the compensation depth. It is computed assuming isostatic compensation. In this case, the geoid anomaly is given by equation (7), where k is the 2-D wavenumber, T the Fourier's transform of the depth anomaly, γ the gravitational constant, g the gravity acceleration, d the mean water depth, t the depth where the compensation occurs and ρ_c and ρ_w the crust and sea water densities, respectively.

$$G(k) = \frac{\gamma}{gk}\left[(\rho_c - \rho_w)e^{-|k|d} - (\rho_c - \rho_w)e^{-|k|(d+t)}\right]T(k). \quad (7)$$

[40] The geoid anomaly is thus composed of two terms (equation (7)): the first one expresses the mass excess due to the uplift of the seafloor, the second one is a negative term related to a deeper density reduction. To obtain the compensation depth (t), we compute the least square difference between this synthetic geoid anomaly grid and the filtered geoid grid.

[41] We compute the compensation depth for each archipelago. Our values are summarized in Table 1 and are discussed and interpreted in the following sections.

4. Polynesian Hot Spots

[42] In the south central Pacific region, corresponding geographically to French Polynesia and Cook Islands, we find a great concentration of volcanism: 14% of the active volcanism is concentrated in an area covering less than 5% of the globe. At least six active hot spots are required to explain the volcanic chains in this region: Macdonald Smt., Arago Smt. and Rarotonga Island in the Cook-Austral volcanic chain, a seamount close to Pitcairn for the Pitcairn-Gambier alignment, Mehetia Island for the Society chain, and a seamount southeast of Fatu Iva for the Marquesas. The Tuamotu volcanic chain (Figure 19a) has the characteristics of both island chains and oceanic plateaus and no recent volcanism is reported there. In order to understand the phenomena at the origin of these chains, a precise characterization of the topographic and geoid anomalies associated with volcanism is required. Next sections show how the anomalies' morphology (displayed in Figure 10) helps to understand and quantify the phenomena at their origin.

4.1. Pitcairn-Gambier

[43] No topographic swell or noticeable geoid anomaly is associated to the Pitcairn-Gambier

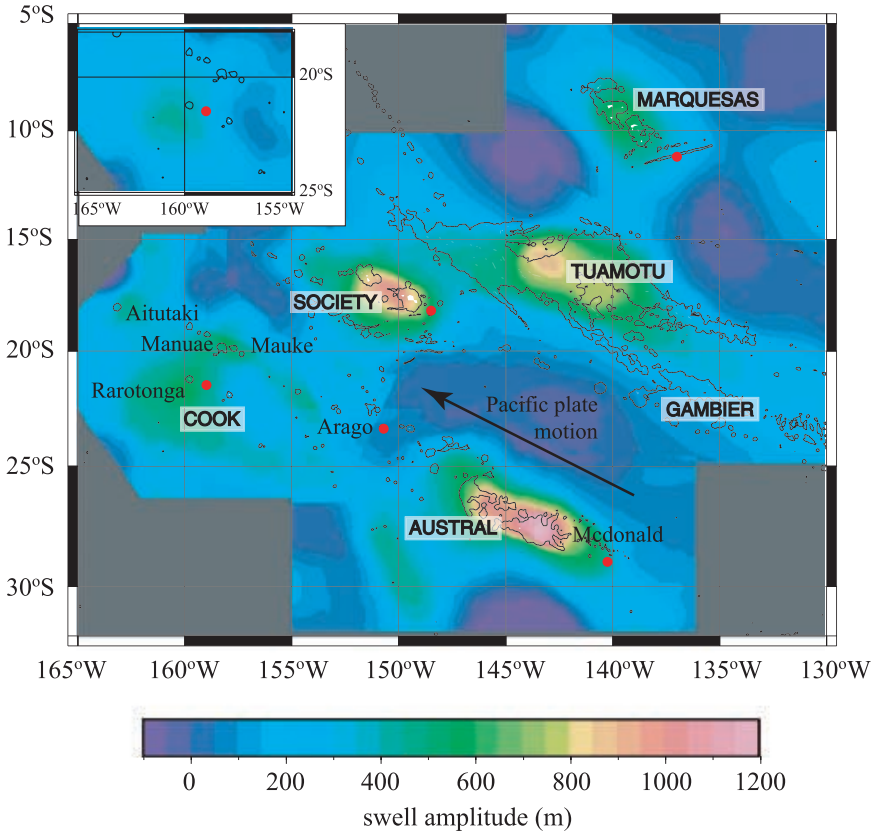

Figure 10. Swell amplitudes (in meters). The general map represents the case in which two swells are found for the Cook Islands. The case when one swell only is found is represented in the top left corner inset. The black line is the 3000 m isobath.

chain at the scale of the alignment and this chain will not be discussed any further.

4.2. Society

4.2.1. Volcanic Chain Description

[44] The Society islands (Figure 11a) are situated between latitudes 16°S and 19°S and longitudes 147°W and 153°W on a seafloor displaying ages between 65 and 95 Ma. They stretch along a 200-km-wide and 500-km-long band orientated in the direction of the present Pacific plate motion: N115 ± 15°. The age progression is uniform from the youngest submarine volcano, Mehetia (0.264 Ma [*Duncan and McDougall*, 1976]), situated at the southeast extremity to the oldest dated island, Maupiti (4.8 Ma [*White and Duncan*, 1996]).

4.2.2. Swell

[45] The topographic anomaly associated with this alignment is shown in Figure 11b. It stretches along the volcanic chain. Its maximal amplitude, 980 m, is reached 30 km northwest of Tahiti, and is not correlated with any volcanic structure. This demonstrates that the volcanoes contribution is efficiently removed by the MiFil method. For this volcanic chain, the swell description corresponds to the one previously reported for hot spot swells, created by the simple interaction of a plume with the lithosphere: the swell's maximum is located 215 kilometers downstream from the active volcanism, the swell stretches along the volcanic chain and subsides along the direction of the plate motion.

4.2.3. Buoyancy Flux

[46] For the Society volcanic chain we find a buoyancy flux of 1.58 ± 0.15 Mg s^{-1}, using V_L = 110 mm yr^{-1}. Previous estimations [*Davies*, 1988; *Sleep*, 1990] are greater, mostly because the authors overestimated the swell volume in not removing completely the volcanoes.

[47] As pointed out by *Courtillot et al.* [2003], several criteria (plume duration, traps at their initiation, rare gas isotopic ratio, Vs at 500 km depth and the buoyancy flux) allow to establish the

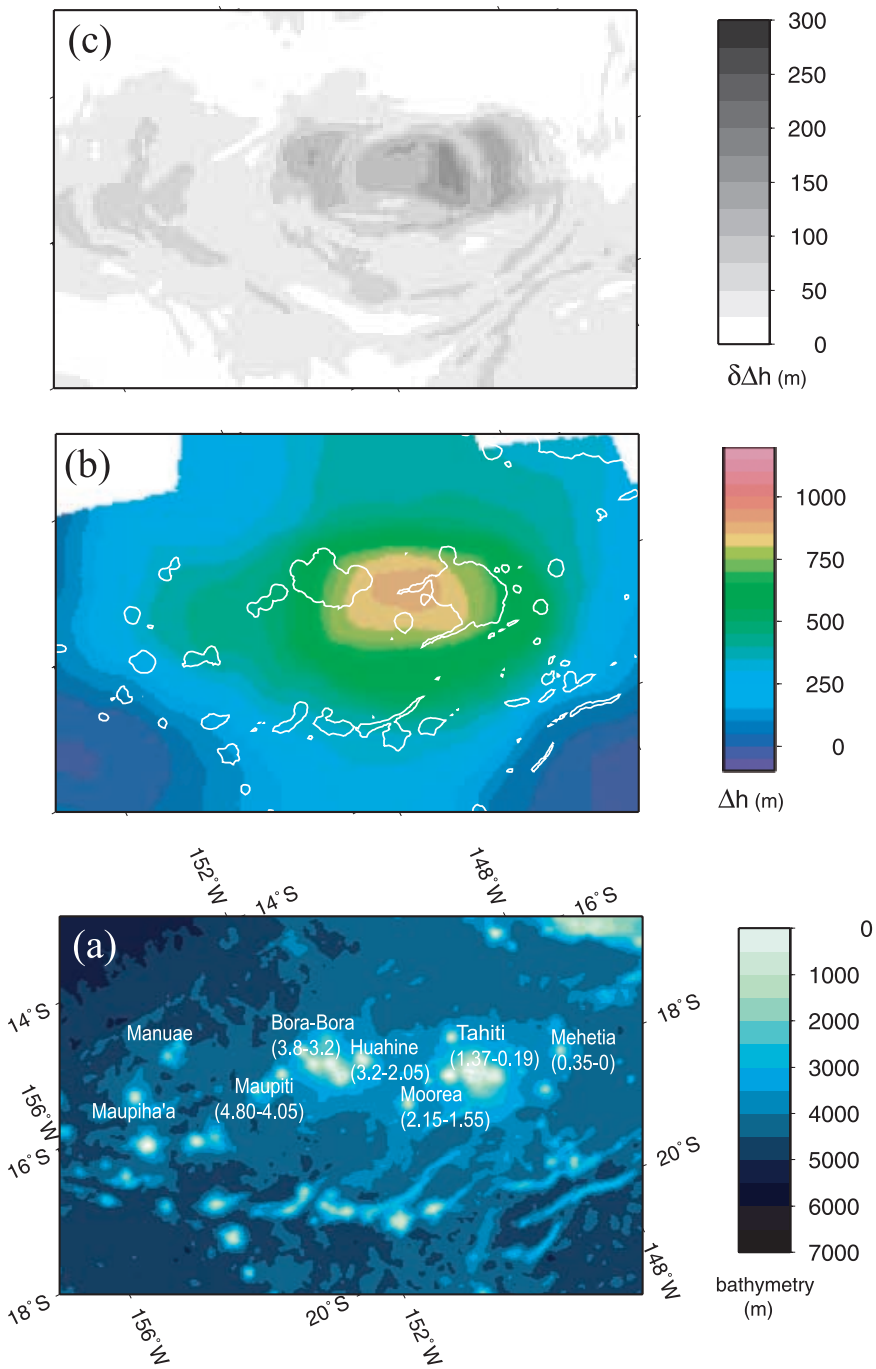

Figure 11. Society volcanic chain. (a) Bathymetry (see text). (b) Hot spot swell. Gray line is the 3000 m isobath. (c) Error on swell determination (see text). All maps are projected along the direction of the present Pacific plate motion (N115°).

depth at which plumes initiate. Deep plumes originate from instabilities out of a thermal boundary layer. The most likely locations are in the transition zone and at the core-mantle boundary. According to *Courtillot et al.*'s [2003] criteria, three types of plumes are found: those which initiate at the CMB (primary plumes), those at the transition zone (secondary hot spots) and the ''Andersonian'' plumes that may be due to a passive response to forms of lithospheric breakup. The buoyancy flux (B) is the most suitable criterion to know which mantle plumes are deep. With a value of B > 1Mg/s, the Society is likely due to a deep plume which is in good agreement with what we already

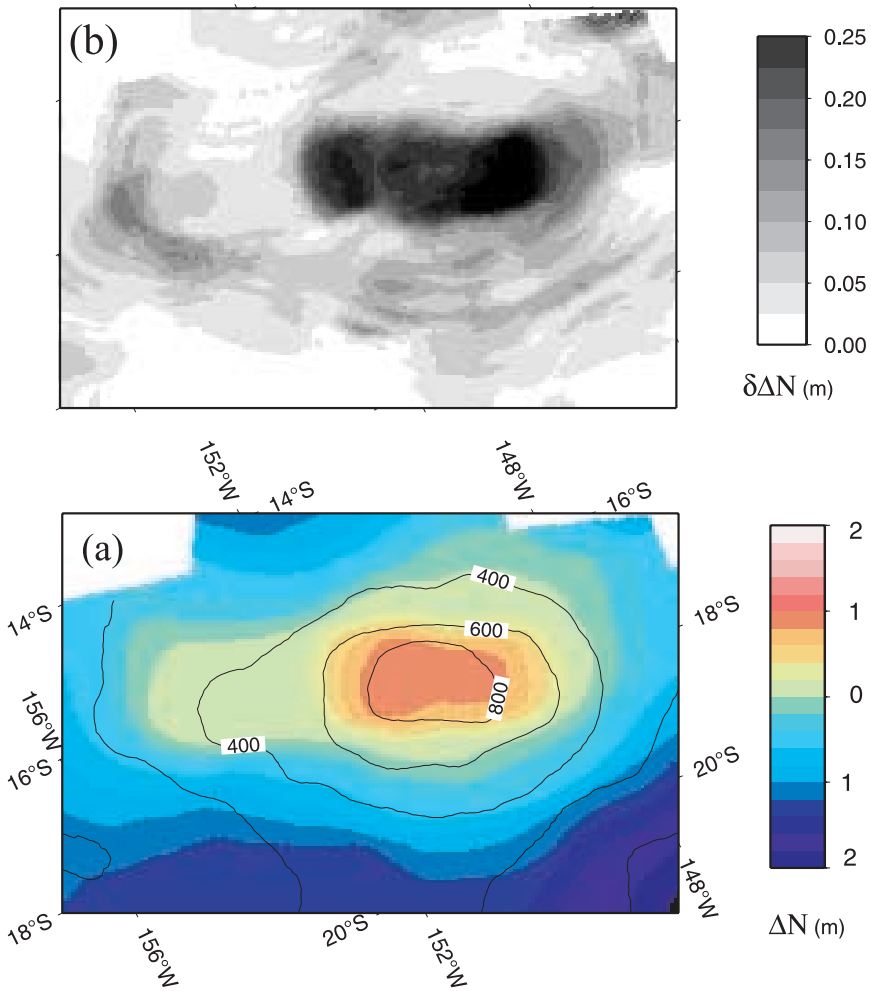

Figure 12. Society volcanic chain. (a) Geoid anomaly, filtered for the swell spatial length scale. Black lines are isovalues of the swell shown in Figure 11b. (b) Error on the geoid due to the filtering method (see text). All maps are projected along the direction of the present Pacific plate motion (N115°).

know for the Polynesian hot spots, supposed to be linked to secondary plumes.

4.2.4. Geoid Anomaly

[48] The geoid anomaly associated with the Society archipelago is shown in Figure 12a. It correlates well with the depth anomaly. As no other phenomenon seems to perturb the plume interaction with the lithosphere, we can then infer the compensation depth $t = 40 \pm 7$ km.

4.3. Marquesas

4.3.1. Volcanic Chain Description

[49] The Marquesas islands stretch between latitudes 7°S and 11°S and longitudes 137°W and 142°W (Figure 13a) on a seafloor displaying ages between 50 and 58 Ma [*Munschy et al.*, 1998]. It seems to be a classical hot spot, with a regular age progression [*Duncan and McDougall*, 1974; *Diraison*, 1991; *Brousse et al.*, 1990] from a seamount southeast of Fatu Iva, which is only a few hundred thousand years old [*Desonie et al.*, 1993], to the Eiao atoll, situated northwest of the chain, displaying an 5.3 Ma age. The direction of this volcanic chain varies according to the authors: *McNutt et al.* [1989] report a N140–146°E direction, whereas *Brousse et al.* [1990] prefer a N160–170°E direction. In all cases, this direction differs from those of the Pacific plate motion.

4.3.2. Swell

[50] The analysis of seismic velocities points out a crustal thickening of several kilometers [*Wolfe et al.*, 1994; *Caress and Chayes*, 1995]. *McNutt and Bonneville* [2000] show that the swell associated

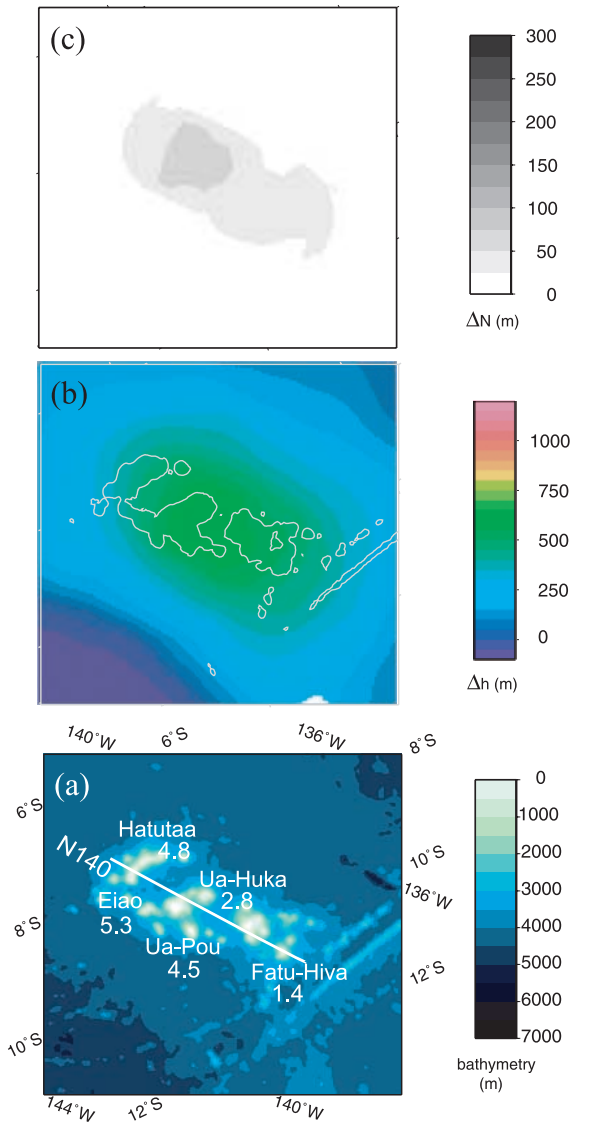

Figure 13. Marquesas volcanic chain. (a) Bathymetry (see text). (b) Hot spot swell. Light gray line is the 3000 m isobath. (c) Error on swell determination (see text). All maps are projected along the direction of the present Pacific plate motion (N115°).

with this alignment is mostly due to underplating. This underplating may contain spatial length scales close to those of the volcanoes. By removing the volcanic edifices, we may also remove a part of the swell that may be related to other phenomena, such as the underplating. We then introduce an error which is hardly quantifiable.

[51] The swell we have determined is shown in Figure 13b. It spreads along the chain axis (if we consider a N140°E direction). Its maximal amplitude (640 m) is reached on the main axis between Nuku Hiva and Hiva Oa, 275 km away from the most recent volcanism. It has an irregular shape since its width is almost constant all along the volcanic alignment. When the swell is due to a classical plume-lithosphere interaction, it is more important near the youngest part of the chain. For the Marquesas, this difference confirms the hypothesis of underplating at its origin. Moreover, it does not subside along the chain direction but along the plate direction. Once again, as we cannot infer which part of the swell corresponds either to the plume effect, or to the underplating one, its study cannot lead to any reliable quantifications.

4.3.3. Geoid Anomaly

[52] The geoid anomaly that we have characterized for this volcanic chain is shown in Figure 14b. The geoid anomaly is shifted 150 km northwest from the chain axis. It is due to the coalescence of two anomalies, clearly visible in the unfiltered geoid anomaly (Figure 14a). One spreads along the volcanic chain and the second is located northwest and stretches along the N150°E direction, between the 46.17 and 50.43 Ma isochrons. Several phenomena can create such a geoid anomaly, not correlated with any topographic anomaly. It may be a plume who has not yet reached the lithosphere. At such a depth, the isostatic compensation is not required. Moreover, a density anomaly will create, whatever its depth, a geoid anomaly. This anomaly can also originate from a dipole located in the lithosphere: a positive density anomaly situated over a negative anomaly. Whatever the case, the phenomenon at the origin of this N150°E orientated anomaly may also have influenced the volcanism emplacement. This remark and the fact that the swell has an unusual shape indicate that these anomalies are due to a sum of phenomena occurring at different depths. Then again, we cannot make any reliable quantifications such as the compensation depth.

4.4. Cook-Austral

4.4.1. General Description

[53] The Cook-Austral volcanic (Figure 15) chain extends to the northwest for more than 2200 km from Macdonald Seamount, an active submarine volcano, to the island of Aitutaki (Figure 15). The chain is composed of eleven islands and two atolls with little area above sea level (the largest is 70 km^2) and around 30 major seamounts. Although oriented roughly in the direction of present Pacific plate motion (11 cm yr^{-1} along a N115° direction), the pattern of both aerial and submarine volcanoes

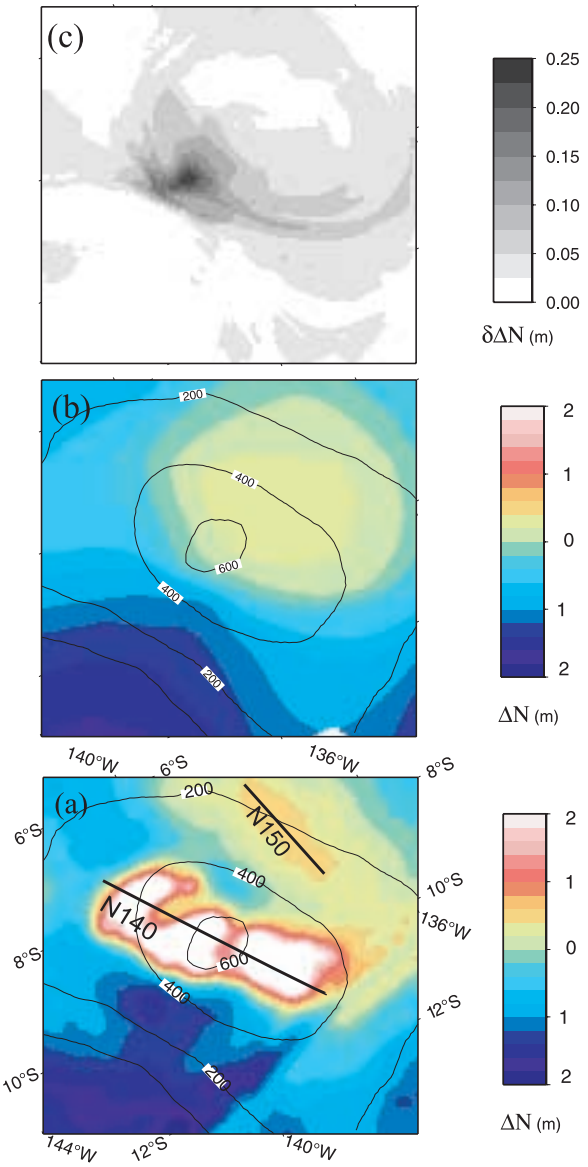

Figure 14. Marquesas volcanic chain. (a) Nonfiltered geoid anomaly. (b) Geoid anomaly, filtered for the swell spatial length scale. Black lines are isovalues of the swell shown on Figure 13b. (c) Error on the geoid due to the filtering method (see text). All maps are projected along the direction of the present Pacific plate motion (N115°).

is rather complex. Morphology and geometry of the island groups suggest the existence of at least two distinct volcanic alignments: the Aitutaki-Mauke Islands group, Rimatara, Rurutu, Tubuai, Raivavae, and President Thiers bank form the northeast alignment; Rarotonga and Mangaia Islands, Neilson bank, Rapa, Marotiri, and Macdonald Seamount, the only known active volcano, form the southwest branch. The age of the oceanic crust along the chain ranges from ca. 35 Ma to 80 Ma [*Mayes et al.*, 1990]. Several good K/Ar or Ar/Ar ages have been obtained for almost all the islands and on seamounts in the Taukina and Ngatemato chains and in the northern Austral region (Figure 15). The Cook-Austral volcanic chain is composed of several volcanic alignments. Recent studies [*Bonneville et al.*, 2002; A. Bonneville et al., Mantle superplume activity and hotspot tracks: New K/Ar ages and geochemical data from the Austral-Cook islands chain, submitted to *Earth and Planetary Science Letters*, 2004] on the Austral part of the region have identified at least three hot spot tracks, from south to north: the Macdonald track from Macdonald seamount (0 Ma) to Mangaia (19 Ma); the young Rurutu track from Arago seamount (0.2 Ma) to Atiu Island (8 Ma) and the old Rurutu track from Raivavae Island (6.5 Ma) to Rurutu Island and nearby seamounts (12 Ma). Concerning Rarotonga, neither the observed age (1.5 Ma), nor the isotopic analysis make it possible to connect it with the above mentioned tracks, it seems to correspond to an isolated plume. The same observation can be made for Aitutaki, an atoll situated less than 250 km north of Rarotonga and dated at 1.2 Ma [*Turner and Jarrad*, 1982]. It is clear that more dated seamounts are needed to propose a valid reconstruction for this northwestern part of the Cook-Austral volcanic chain.

[54] Two depth anomalies are clearly observed: one centered on Rarotonga Island and the other one linked to the southwestern branch with Macdonald seamount. Note that northern Austral Islands are not associated with any depth or geoid anomalies.

4.4.2. Cook Volcanic Chain

[55] For this chain, the characteristics of the depth anomaly change completely according to the filtering parameters. This is illustrated in Figure 16, where we show the swell obtained with two different filters. In the first case, we find an almost circular swell centered on the south of Rarotonga. In the second case (filter 2), we find two parallel swells: one north, centered on the Atiu-Mitiaro-Mauke islands and a second south, elongated along a subparallel axis orientated in the direction of the present Pacific plate motion, 100 km south of Rarotonga.

[56] On the profile shown in Figure 17, we can see that this duplication is not an artifact of the filtering method but that there are indeed two swells of different spatial length scale that are superimposed:

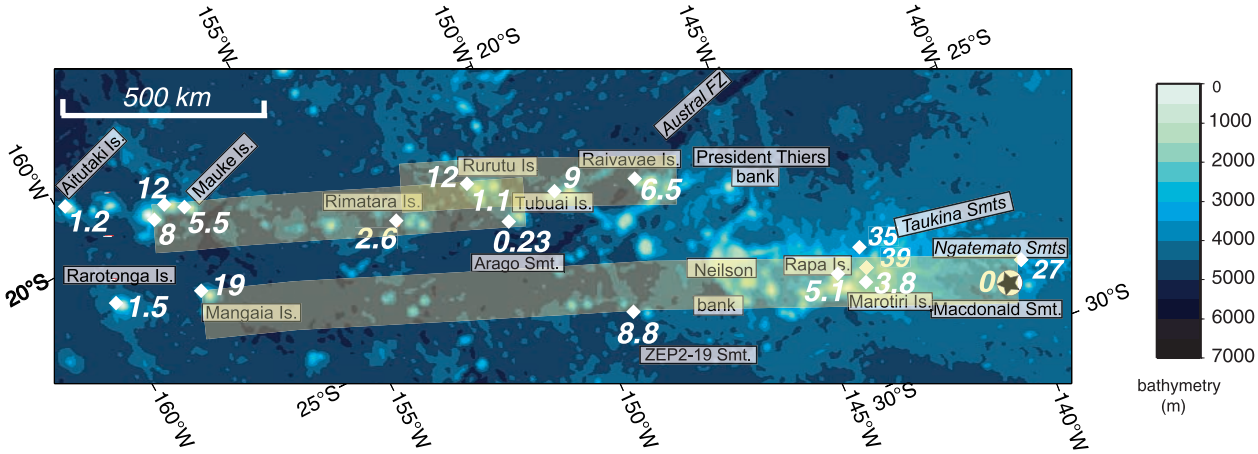

Figure 15. Bathymetry of the Cook-Austral volcanic chain, projected along the direction of the present Pacific plate motion (N115°). The light green ribbons represent the "old Rurutu," "young Rurutu," and Macdonald hot spot tracks as proposed by *Bonneville et al.* [2002]. Note that volcanoes are often not located exactly on the middle of a track, which could indicate the importance of lithospheric control rather than a change in the location of the magmatic source. The volcanism ages are in Ma.

the one with the largest spatial length scale, centered on Rarotonga, shown in Figure 16a, the other centered on the Atiu-Mitiaro-Mauke islands, shown in Figure 16b. If we want to quantify the plume effect on the lithosphere, we have then to compute the buoyancy flux from the swell obtained by filter 1. We obtain in this case $B = 0.92 \pm 0.09$ Mg s^{-1}.

[57] The filtered geoid anomaly is shown in Figure 16c. We tried both filters to characterize the geoid anomaly and in this case, its morphology is not very sensitive to the filtering parameters. There are also two positives anomalies: the most important has an almost circular shape and is situated a hundred kilometers southwest of Rarotonga; the other one has an elongated form and stretches along the 158°W longitude, between latitudes 21.5 and 19°S.

4.4.3. Northern Austral Islands

[58] The northwesternmost part of the Austral chain is associated neither to a depth anomaly nor to a geoid anomaly. A reason that could explain these observations is that the emplacement of the latest volcanism is favored by a lithospheric weakness left in the lithosphere by the previous stages and not to the "classical" dynamic uplift of a plume [*Bonneville et al.*, 2002].

4.4.4. Southern Austral Chain

[59] The swell obtained for the southern part of the Austral islands is shown in Figure 18a. It has an irregular shape: a part of the swell stretches along the axis connecting Macdonald and Rapa; an other part is shifted northwest and is not correlated with any recent volcanic structure. This peculiar morphology indicates that the topographic anomaly is the sum of several physical phenomena, the most important being probably the thick limestone layers above the old guyots comprised between Neilson Bank to the south and President Thiers bank to the north. The spatial length scale of the swell is about 1250 km. The maximal amplitude reaches 1220 m and is located 375 km from the active volcanism (Macdonald).

[60] For this region we also show the geoid anomaly on Figure 18b. The geoid anomaly that reaches a maximum of 0.9 m and is well correlated with the topographic swell. We computed a $t = 20 \pm 5$ km compensation depth, but as the anomalies display irregular shapes, we cannot affirm that this value corresponds to the plume effect and not to other more superficial phenomena.

4.5. Tuamotu

4.5.1. Volcanic Chain Description

[61] Situated between the Marquesas and Austral Fracture Zones, the Tuamotu volcanic chain (Figure 19a) has the characteristics of both island chains and oceanic plateaus. The sixty atolls composing the Tuamotu fall under two parallel alignments orientated N115°E (red dashed line in

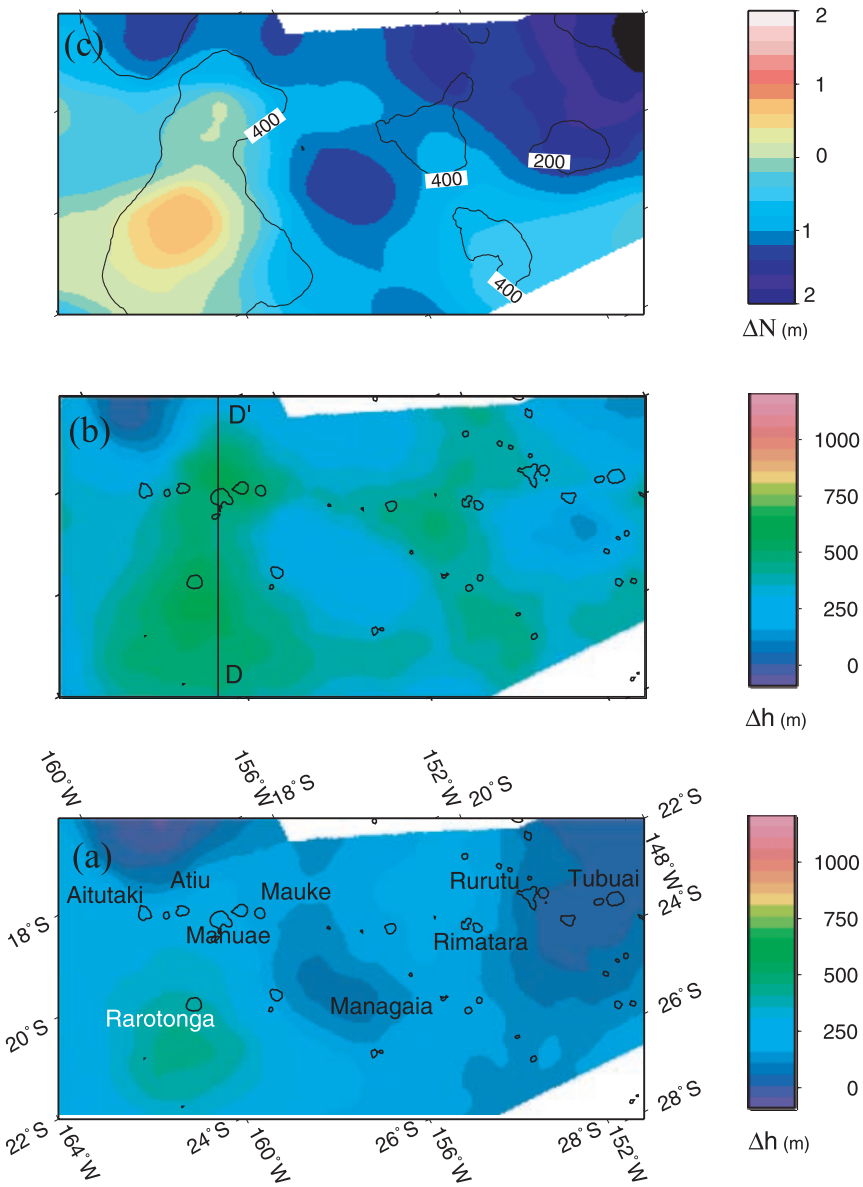

Figure 16. Cook volcanic chain. (a) Hot spot swell obtained with filter 1 (r = 15 km, R = 175 km). (b) Same with filter 2 (l = 5 km, R = 120 km); black line is the 3000 m isobath. The profile DD' will be discussed later. (c) Geoid anomaly, filtered for the swell spatial length scale using filter 2. Black lines are isovalues of the swell filtered with filter 2. All maps are projected along the direction of the present Pacific plate motion (N115°).

Figure 19b), thus suggesting a hot spot origin [*Morgan*, 1972; *Okal and Cazenave*, 1985]. They are superimposed on a large plateau capped with sediments, limestone and basalt layers. The origin of the plateau still remains controversial. *Ito et al.* [1995] propose a scenario according to which the northern segment of the Pacific-Farallon spreading center propagates southward in an inner pseudofault and a failed rift and northward in an outer pseudofault (see Figure 19a). The southern discontinuities would enclose a block of lithosphere transferred from the Farallon plate to the Pacific plate, called the "lithospheric transfer zone" by *Hey et al.* [1986] (hachured in Figure 19a). This zone of discontinuity focuses volcanism along the Tuamotu Plateau, channels the magma uplift and is then responsible for the plateau shape and morphology.

4.5.2. Swell

[62] The interpretation of the swell morphology (Figure 19b) is in this case difficult since we cannot remove the plateau component. There is

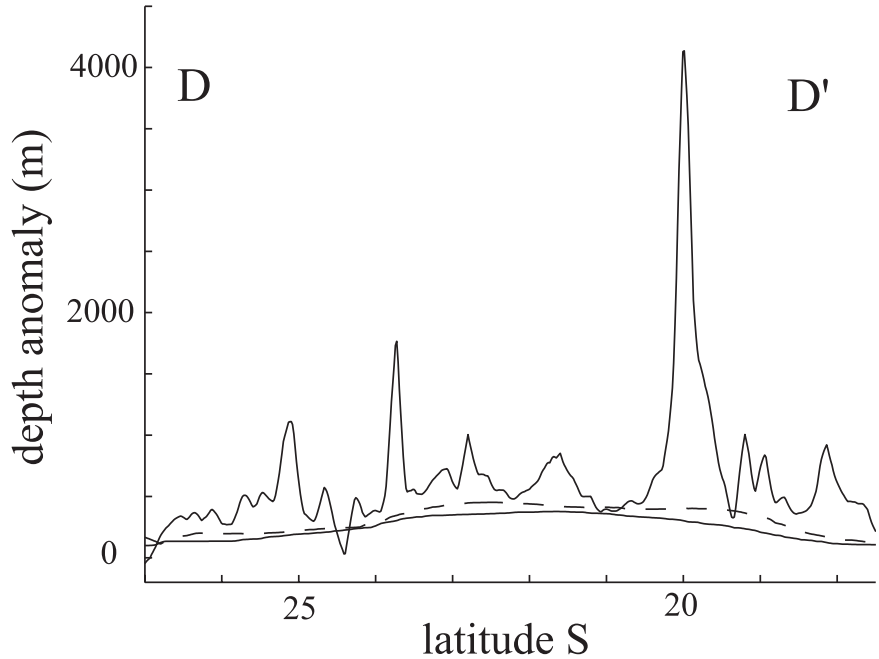

Figure 17. Depth anomaly (solid black line), swell obtained with filter 1 (dashed line) and filter 2 (solid line) for the Cook-Austral volcanic chain. The profile DD′ is located in the Cook volcanic chain (see Figure 16b).

only one seismic profile across this volcanic chain [*Ito et al.*, 1995] (Figure 19a), showing great variations in the thicknesses of the limestone and basalt layers. Therefore we cannot infer the structure and extension of the plateau. We can just make qualitative interpretations. The swell that we characterized (Figure 19b) is a composite feature: to the west, a large horizontal band stretches between longitudes 145 and 150°W, at the 16°S latitude with a 500 m amplitude. It is situated between the Society and Tuamotu volcanic chains. To the east, one finds a swell orientated along the direction of the present Pacific plate motion: N115 ± 15°. Its maximum (890 m) corresponds to the jump between the two volcanic segments. This swell continues after the end of the Tuamotu volcanic chain and seems to be in continuation of the Easter alignment.

4.5.3. Geoid Anomaly

[63] The filtered geoid anomaly is shown in Figure 19c, where we have also reported the isovalues of the swell (gray lines). It is partially correlated with the depth anomaly and is composed of two features with the same orientation: the western geoid anomaly correlated with the east-west oriented swell whose amplitude reaches 500 m and the eastern anomaly corresponding to the transition between the two volcanic alignments and to the maximum amplitude of the swell.

5. Discussion

[64] The Society is the only "classical" volcanic alignment: its trace is parallel to the direction of the present Pacific plate motion and volcanic ages increase regularly to the northwest. The topography and geoid anomalies stretch symmetrically along the main axis. The swell morphology is classical with an important upwelling of the seafloor near the active volcanism. The swell maximum and the active volcanism are separated in space by 215 kilometers and in time by 2 m.y.. Northwest of the maximum, the swell subsides along the direction of the Pacific plate motion. No other superficial phenomenon seems to perturb the plume-lithosphere interaction.

[65] The Marquesas volcanic chain also corresponds to some of these characteristics since the volcanism age progression is regular and since the swell spreads symmetrically along the alignment axis, reaching its maximum 275 km from the most recent volcanism. However, the swell morphology does not correspond to a classical plume-lithosphere interaction: the swell width is constant along the volcanic alignment and its subsidence, which occurs a few hundred kilometers to the end

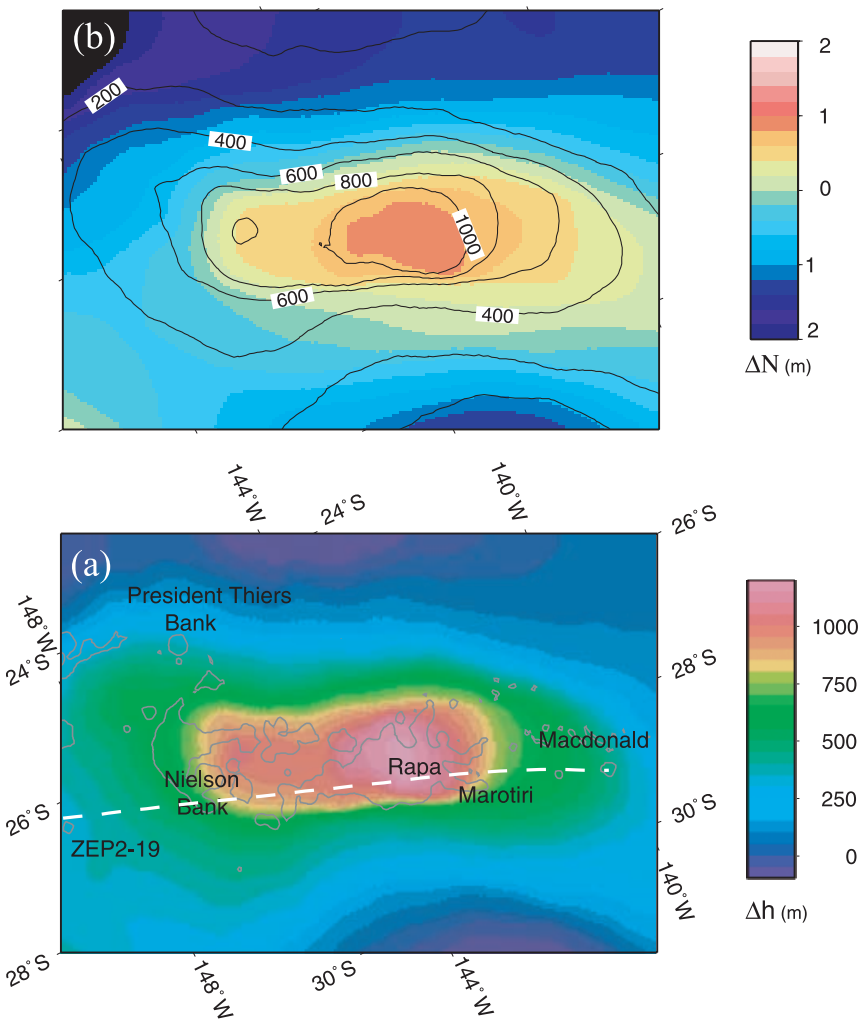

Figure 18. Southern part of the Austral volcanic chain. (a) Hot spot swell. Light gray line is the 3000 m isobath. The white dashed line represents the central axis of the Macdonald hot spot track shown in Figure 15. (b) Geoid anomaly, filtered for the swell spatial length scale. Black lines are isovalues of the swell. All maps are projected along the direction of the present Pacific plate motion (N115°).

of the volcanic alignment, happens along the direction of the Pacific plate, and not along the direction of the volcanic chain. Moreover, *McNutt and Bonneville* [2000] show that this topographic anomaly can be explained by an underplated body. We also show that there is a geoid anomaly, along the N150° direction, not correlated with any topographic anomaly. The phenomenon responsible for this anomaly may also have influenced the volcanism emplacement.

[66] The Cook-Austral volcanic chain present a different and much more complicate scheme of evolution. For the southern part of this alignment, we note that the distance between the swell maximum and the active volcanism (Macdonald seamount) is 373 km, roughly two times more than for the Marquesas and the Society volcanic chains. This could be due to the presence of thick limestone deposits to the west not correctly taken into account in the initial sediment correction. It may be also explained if assuming that the plume reaches the end of its activity and is no more strong enough to influence the thermal structure of the lithosphere. This latter hypothesis is corroborated by *Adam*'s [2003] study of the elastic thickness which shows a localized thinning of the lithosphere beneath Mangaia, ZEP2-19 Smt. and Rapa, whereas Macdonald loaded a lithosphere of normal thickness owing to its age.

[67] For the Cook region, according to the filtering parameters, one or two swells appear: a roughly circular swell located slightly south of Rarotonga

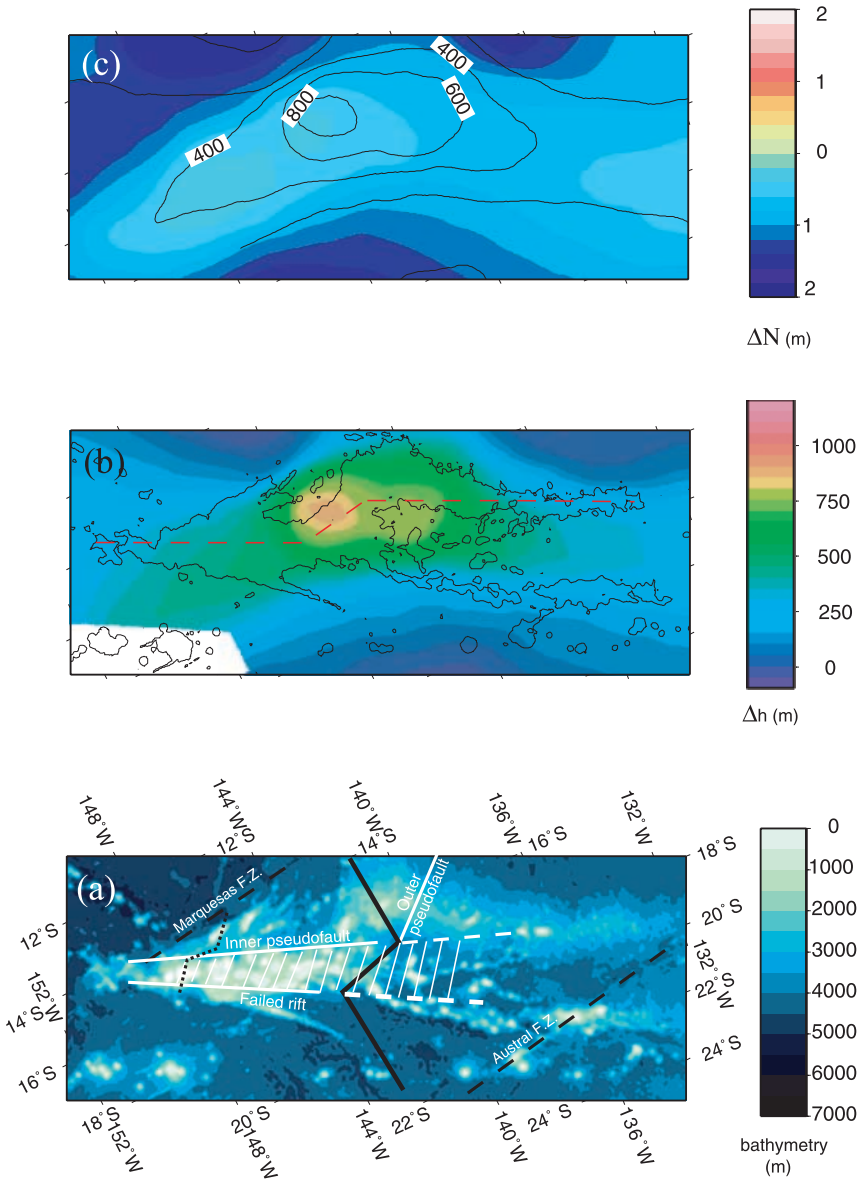

Figure 19. Tuamotu volcanic chain. (a) Bathymetry (see text). The thickest black lines represent the geometry of the Pacific-Farallon spreading center at time 50 Ma, which propagated southward in an inner pseudofault and a failed rift, and northward in an outer pseudofault (white lines). The hachured area represents a part of the lithosphere transferred from the Farallon to the Pacific plate. The dotted black line represents the only refraction seismic profile made across the chain [*Ito et al.*, 1995]. (b) Hot spot swell. The black line is the 3000 m isobath. The red dashed line represents the main axis of elongation of the two segments of the Tuamotu chain. (c) Geoid anomaly, filtered for the swell spatial length scale. Black lines are isovalues of the swell (Figure 19b). All maps are projected along the direction of the present Pacific plate motion (N115°).

and a swell focused on Atiu-Mitiaro-Mauke. One can note that, despite the coalescence of these 2 anomalies nothing can be concluded on the link between these volcanic episodes.

[68] The morphology of the Rarotonga swell is also peculiar since the almost circular swell does not show any subsidence along the direction of the plate movement. It may be due to the interaction of the plate with a young plume who just reached the lithosphere. This hypothesis is consistent with the surface observations: no other older volcano is associated with this trace.

[69] The Cook-Austral region stands out because apparently the lithospheric control plays a major role. We found no "classical" swell, whose description corresponds to the one previously reported

[*Crough*, 1983]. On the other hand, there are volcanic alignments not associated with any swell, as the one including Raivavae, Tubuai and Rurutu, whose tectonic history involves the superposition of different volcanic stages.

[70] More generally, the study of the correlation between the geoid and topographic anomalies provides information on the compensation depth. The plume magma, hotter and less dense than the surrounding environment, raises the oceanic seafloor so as to obtain an isostatic equilibrium. For all the volcanic chains, we found compensation depths between 20 and 40 km. But as we have noticed before, the correlation is not always obvious. In our region, several phenomena get mixed up and it is important to isolate each of them if we want to infer the characteristics of the plume at the origin of the volcanic alignment, such as the compensation depth and/or the buoyancy flux. The values we infer for the Society volcanic chain, the only "classical" alignment are the only reliable values. Although we find here a smaller value that in previous studies, the buoyancy flux indicates a deep plume at the origin of this alignment [*Courtillot et al.*, 2003]. This assertion is in agreement with *Niu et al.*'s [2002] results, who show from the reflection of the shear waves on the 410 and 660 km discontinuities that the thickness of the transition zone is 25 km lower on an area situated northwest of Tahiti and whose diameter is less than 500 km.

[71] The ninth column in Table 1 indicates the volume associated with the swell, calculated between a reference floor at $z = 0$ and the surface of the depth anomaly. This volume can be directly linked to the buoyancy flux of the hot rising plume creating the swell, and thus give information on the plume strength [*Sleep*, 1990]. The most important swell of French Polynesia is the Society one. According to *Courtillot et al.* [2003] criterion, most of the Polynesian hot spots can be considered as deep ones. However they remain small compared to the Hawaiian swell ($V = 9.53 \times 10^5$ km^3 [*Vidal and Bonneville*, 2004]). Many plumes are concentrated in French Polynesia, but they are much less important than the isolated Hawaiian plume.

6. Conclusion

[72] We have demonstrated that the MiFil method of spatial filtering is particularly adapted to the characterization of hot spot swells. Its main advantages are that it does not require any assumption on the shape, spatial length scale and location of the studied features and that it efficiently removes the volcanic edifices. This method brings new information on the transversal spreading of topographic swells and on their precise morphology.

[73] Application to volcanic chains of the south central Pacific leads to a better understanding of the tectonics and volcanism emplacement of the zone. The Society is the only "classical" hot spot that corresponds to the simple interaction of a plume with the lithosphere. In this case, the buoyancy flux indicates a rather deep plume with the corresponding seafloor swell compensated at 40 km depth.

[74] The Marquesas volcanic chain also corresponds to some of these characteristics since the volcanism age progression is regular and since the swell spreads symmetrically along the alignment axis. However, the swell morphology does not correspond to a classical plume-lithosphere interaction.

[75] For the Tuamotu and Cook-Austral volcanic chains, no reliable quantification can be made because the depth and geoid anomalies are caused by several phenomena occurring at different depths that cannot be separated.

Acknowledgments

[76] C.A. was supported from a grant of the ZEPOLYF program funded by the French Ministry of Research and by the government of French Polynesia. The authors wish to thank Michel Diament and Paul Wessel for their careful remarks during the preparation of this paper. Our manuscript has been greatly improved by the comments of Peter van Keken, Shijie Zhong, and an anonymous reviewer. This is IPGP contribution 2016.

References

Adam, C. (2003), Signature topographique et gravimétrique des panaches du manteau dans le Pacifique, Ph.D. thesis, 221 pp., Inst. de Phys. du Globe de Paris/Univ. de Polynésie Française, Paris.

Bendat, J., and A. Piersol (1986), *Random Data: Analysis and Procedure Analysis*, John Wiley, Hoboken, N. J.

Bonneville, A., R. L. Suavé, L. Audin, V. Clouard, L. Dosso, P.-Y. Gillot, P. Janney, K. Jordahl, and K. Maamaatuaiahutapu (2002), Arago Seamount: The missing hotspot found in the Austral Islands, *Geology*, *30*, 1023–1026.

Brousse, R., G. Barsczus, H. Bellon, J.-M. Cantagrel, C. Diraison, H. Guillou, and C. Leotot (1990), Les Marquises (Polynésie Française): Volcanologie, géochronologie, discussion d'un modèle de point chaud, *Bull. Soc. Geol. France*, *6*, 933–949.

Caress, D., and D. Chayes (1995), New software for processing data from side-scan-capable multibeam sonars, in *Oceans'95: Challenges of Our Changing Global Environment*, vol. 2, pp. 997–1000, Mar. Technol. Soc., MTS-IEEE, Washington, D. C.

Cazenave, A., and K. Dominh (1987), Global relationship between oceanic geoid and seafloor depth: New results, *Geophys. Res. Lett.*, *14*, 1–4.

Courtillot, V., A. Davaille, J. Besse, and J. Stock (2003), Three distinct types of hotspots in the Earth's mantle, *Earth Planet. Sci. Lett.*, *205*, 295–308.

Crough, S. (1978), Thermal origin of mid-plate hot-spot swells, *Geophys. J. R. Astron. Soc.*, *55*, 451–469.

Crough, S. (1983), Hotspot swells, *Annu. Rev. Earth Planet. Sci.*, *11*, 165–193.

Davies, G. (1988), Ocean bathymetry and mantle convection, 1, Large-scale flow and hotspots, *J. Geophys. Res.*, *93*, 10,467–10,480.

Desonie, D., R. Duncan, and J. Natland (1993), Temporal and geochimical variability of volcanic products of the Marquesas hotspot, *J. Geophys. Res.*, *98*, 17,649–17,665.

Didden, N., and T. Maxworthy (1982), The viscous spreading of plane and axisymetric gravity currents, *J. Fluid Mech.*, *121*, 27–42.

Diraison, C. (1991), Le volcanisme aérien des archipels polynésiens de la Société, des Marquises et des Australes-Cook, Ph.D. thesis, 413 pp., Université de Bretagne Occidentale, Brest, France.

Duncan, R., and I. McDougall (1974), Migration of volcanism with time in the Marquesas Islands, French Polynesia, *Earth Planet. Sci. Lett.*, *21*, 414–420.

Duncan, R., and I. McDougall (1976), Linear volcanism in French Polynesia, *J. Volcanol. Geotherm. Res.*, *1*, 197–227.

Hey, T., M. Kleinrock, S. Miller, T. Atwater, and R. Searle (1986), Sea Beam/Deep-Tow investigation of an active oceanic propagating rift system, Galapagos 95.5°W, *J. Geophys. Res.*, *91*, 3369–3393.

Huppert, H. (1982), The propagation of two-dimensional and axisymetric viscous gravity currents over a rigid horizontal surface, *J. Fluid Mech.*, *121*, 43–58.

Ito, G., M. McNutt, and R. Gibson (1995), Crustal structure of the Tuamotu Plateau, 15°S, and implications for its origin, *J. Geophys. Res.*, *100*, 8097–8114.

Jordahl, K., D. Caress, M. McNutt, and A. Bonneville (2004), Seafloor morphology of the South Pacific Superswell region, in *Oceanic Hot Spots*, edited by R. Hekinian, Springer, New York.

Mayes, C., L. Lawver, and D. Sandwell (1990), Tectonic history and new isochron chart of the South Pacific, *J. Geophys. Res.*, *95*, 8543–8567.

Mazzega, P., M. Bergé-Nguyen, A. Cazenave, and P. Schaeffer (1997), Mean sea surface and gravity anomaly maps from ERS 1 and GEOSAT altimetry, paper presented at Joint Assembly of IAMAS-IAPSO, Int. Assoc. of Meteorol. and Atmos. Sci., Melbourne, Australia.

McNutt, M., and A. Bonneville (2000), A shallow, chemical origin for the Marquesas Swell, *Geochem. Geophys. Geosyst.*, *1*, doi:10.1029/1999GC000028.

McNutt, M., and K. Fischer (1987), The South Pacific Superswell, in *Seamounts, Islands and Atolls*, *Geophys. Monogr. Ser.*, vol. 43, edited by B. Keating et al., pp. 25–34, AGU, Washington, D. C.

McNutt, M., K. Fischer, S. Kruse, and J. Natland (1989), The origin of the Marquesas fracture zone ridge and its implications for the nature of hot spots, *Earth Planet. Sci. Lett.*, *91*, 381–393.

Menard, H. (1973), Depth anomalies and the bobbing motion of drifting islands, *J. Geophys. Res.*, *78*, 5128–5137.

Morgan, W. (1971), Convection plumes in the lower mantle, *Nature*, *230*, 42–43.

Morgan, W. (1972), Plate motion and deep mantle convection, *Geol. Soc. Am. Bull.*, *132*, 7–22.

Müller, D., W. Roest, J.-Y. Royer, L. Gahagan, and J. Sclater (1997), Digital isochrons of the world's ocean floor, *J. Geophys. Res.*, *102*, 3211–3214.

Munschy, M., C. Antoine, G. Guille, and H. Guillou (1998), La croûte océanique et les points chauds de la Polynésie française (Océan Pacifique central), *Geol. France*, *3*, 5–13.

Niu, F., S. Solomon, P. Silver, D. Suetsugu, and H. Inoue (2002), Mantle transition-zone structure beneath the South Pacific Superswell and evidence for a mantle plume underlying the Society hotspot, *Earth Planet. Sci. Lett.*, *198*, 371–380.

Okal, E., and A. Cazenave (1985), A model for the plate tectonic evolution in the East-central Pacific based on SEASAT investigations, *Earth Planet. Sci. Lett.*, *72*, 99–116.

Parker, R., and D. Oldenburg (1973), Thermal model of ocean ridges, *Nature Phys. Sci.*, *242*, 137–139.

Parsons, B., and J. Sclater (1977), An analysis of the variation of ocean floor bathymetry and heat flow with age, *J. Geophys. Res.*, *82*, 803–827.

Ribe, N., and A. Watts (1982), The distribution of intraplate volcanism in the Pacific Ocean: A spectral approach, *Geophys. J. R. Astron. Soc.*, *71*, 333–362.

Rousseeuw, P., and A. Leroy (1987), *Robust Regression and Outlier Detection*, 329 pp., John Wiley, Hoboken, N. J.

Sclater, J., and J. Francheteau (1970), The implication of terrestrial heat flow observations on current tectonic and geochemical models of the crust and upper mantle of the Earth, *Geophys. J. R. Astron. Soc.*, *20*, 509–542.

Sichoix, L. (1997), Le volcanisme de la Polynésie française: Caractérisation des points chauds et du superbombement à partir d'une nouvelle synthèse bathymétrique, Ph.D. thesis, 297 pp., Univ. Française du Pac., Tahiti.

Sichoix, L., A. Bonneville, and M. McNutt (1998), The seafloor swells and Superswell in French Polynesia, *J. Geophys. Res.*, *103*, 27,123–27,133.

Sleep, N. (1990), Hotspots and mantle plumes: Some phenomenology, *J. Geophys. Res.*, *95*, 6715–6736.

Smith, W. (1990), Marine geophysical studies of seamounts in the Pacific Ocean Basin, Ph.D. thesis, Columbia Univ., New York.

Smith, W. (1993), On the accuracy of digital bathymetric data, *J. Geophys. Res.*, *98*, 9591–9603.

Smith, W., and D. Sandwell (1997), Global sea floor topography from satellite altimetry and ship depth soundings, *Science*, *277*, 1956–1962.

Stein, C., and S. Stein (1992), A model for the global variation in oceanic depth and heat flow with lithospheric age, *Nature*, *359*, 123–129.

Telford, W., L. Geldart, R. Sheriff, and D. Keys (1986), *Applied Geophysics*, 860 pp., Cambridge Univ. Press, New York.

Turcotte, D., and E. Oxburgh (1967), Finite amplitude convective cells and continental drift, *J. Fluid Mech.*, *28*, 29–42.

Turner, D., and R. Jarrad (1982), K-Ar dating of the Cook-Austral island chain: A test of the hot-spot hypothesis, *J. Volcanol. Geotherm. Res.*, *12*, 187–220.

Vidal, V., and A. Bonneville (2004), Variations of the Hawaiian hot spot activity revealed by variations in the magma production rate, *J. Geophys. Res.*, *109*, B03104, doi:10.1029/2003JB002559.

Watts, A., and S. Daly (1981), Long-wavelength gravity and topography anomalies, *Annu. Rev. Earth Planet. Sci.*, *9*, 415–448.

Watts, A., U. ten Brink, P. Buhl, and T. Brocher (1985), A multichannel seismic study of lithospheric flexure across the Hawaiian-Emperor seamount chain, *Nature*, *315*, 105–111.

Wessel, P. (1993), Observational constraints on models of the Hawaiian hot spot swell, *J. Geophys. Res.*, *98*, 16,095–16,104.

Wessel, P. (1998), An empirical method for optimal robust regional-residual separation of geophysical data, *J. Math. Geol.*, *30*, 391–408.

Wessel, P., and W. Smith (1991), Free software helps map and display data, *Eos Trans. AGU*, *72*, 441.

White, W. M., and R. A. Duncan (1996), Geochemistry and geochronology of the Society Islands: New evidence for deep mantle recycling, in *Isotope Studies of Crust-Mantle Evolution*, edited by S. R. Hart and A. Basu, pp. 183–206, AGU, Washington, D. C.

Wilson, J. (1963), A possible origin of the Hawaiian Islands, *Can. J. Phys.*, *41*, 863–870.

Wolfe, C., M. McNutt, and R. Detrick (1994), The Marquesas archipelagic apron: Seismic stratigraphy and implications for volcano growth, mass wasting, and crustal underplating, *J. Geophys. Res.*, *99*, 13,591–13,608.